The Rise of 212 MAX Phase Borides: DFT Insights into the Physical Properties of Ti$_2$PB$_2$, Zr$_2$PbB$_2$, and Nb$_2$AB$_2$ [A = P, S] for Thermomechanical Applications

Md. Ashraf Ali,* Md. Mukter Hossain, Md. Mohi Uddin, A. K. M. Azharul Islam, and Saleh Hasan Naqib*

ACCESS | Metrics & More | Article Recommendations | SI Supporting Information

ABSTRACT: In this article, *ab initio* calculations of unexplored Ti$_2$PB$_2$, Zr$_2$PbB$_2$, and Nb$_2$AB$_2$ [A = P, S] were performed wherein Ti$_2$PB$_2$ along with its 211 boride phase Ti$_2$PB was predicted for the first time. The stability was confirmed by calculating the formation energy, phonon dispersion curve, and elastic stiffness constants. The obtained elastic constants, elastic moduli, and Vickers hardness values of Ti$_2$PB$_2$, Zr$_2$PbB$_2$, and Nb$_2$AB$_2$ [A = P, S] were found to be significantly larger than those of their counterparts 211 borides and carbides. The studied compounds are brittle, like most MAX and MAB phases. The electronic band structure and density of states revealed the metallic nature of the titled borides. Several thermal parameters were explored, certifying the suitability of Ti$_2$PB$_2$, Zr$_2$PbB$_2$, and Nb$_2$AB$_2$ [A = P, S] to be used as efficient thermal barrier coating materials. The response of Ti$_2$PB$_2$, Zr$_2$PbB$_2$, and Nb$_2$AB$_2$ [A = P, S] to the incident photon was studied by computing the dielectric constant (real and imaginary parts), refractive index, absorption coefficient, photoconductivity, reflectivity, and energy loss function. In this work, we have explored the physical basis of the improved thermomechanical properties of 212 MAX phase borides compared to their existing carbide and boride counterparts.
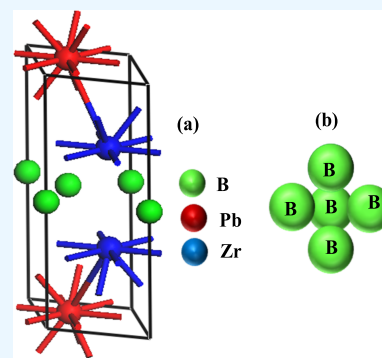
1. INTRODUCTION

The demand for novel materials with a better demonstration of their performances in various applications is increasing day by day in association with the advancement of technology. One of the best ways to achieve this goal is the prediction and/or synthesis of novel materials in addition to the existing ones that are used in various technological applications. Since the practical use of MAX phase results due to their peculiar physical properties, the prediction, synthesis, and the study of newly synthesized MAX phase materials have received huge interest from both applications and basic research points of view.[1] The term MAX represents a layered class of solids in which M represents the transition metal group, A represents the IIIA or IVA group in the periodic table, and X is a C/N/B atom.[2−8] Despite the metallic nature of the MAX phase materials, they are also potential candidates for use as an alternative to high-temperature materials because of their ceramic-like characteristics.[1,4,5,9,10] A long list of their potential applications can be found elsewhere.[1,5,11−13]

However, the main focus for the discovery of a new MAX phase was limited due only to the extension of either the M element or the A element[14−23] or reporting of the MAX phase alloys by the combination of M, M′, and A, A′ atoms; M, M′ = Ti, Zr, Hf, Ta, ...; A, A′ = Al, Ga, Si, Ge, P, ...[24−33] The atom X was recognized as either C/N for a long time before the groundbreaking work of Khazaei et al.[5] where they proposed B

as an X element. Before this proposal, very few attempts were made to extend the MAX phase family by tuning the X elements in comparison with the attempts taken to extend by choosing the M and/or A element(s) for the same. Both the physical and chemical characteristics of B, as well as B-containing compounds, convey the prospects of the MAX phase borides by replacing C/N with boron.[34] Recently, such systems have been synthesized and are already listed as promising members of the MAX phases. Significant attention has also been paid to these MAX phase borides.[6−8,35−43] The first report on the hypothetical MAX phase borides [M$_2$AlB (M = Sc, Ti, Cr, Zr, Nb, Mo, Hf, or Ta)] was published by Khazaei et al.[6] where the trend in the electronic structures of the phase stability has been investigated. Gencer and Surucu[43] reported the electronic and vibrational properties of Ti$_2$SiB. A predictive study of M$_2$AlB (M = V, Nb, Ta) borides was performed by Surucu et al.[44] The first synthesis of the M$_2$SB (M = Zr, Hf, and Nb) borides phase was carried out by Rackl et al.[7,38] Chakraborty et al.[39] predicted the
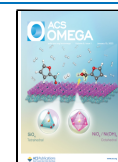
V$_2$AlB boride by B substitution in place of C in the V$_2$AlC. A DFT study of M$_2$AB (M = Ti, Zr, Hf; A = Al, Ga, In) compounds was carried out by Surucu[40] in which the structural, electronic, elastic anisotropy, and lattice dynamical properties were considered. We have performed a comprehensive investigation of the synthesized borides M$_2$SB (M = Zr, Hf, and Nb) in our earlier report,[41] where the physical properties of borides were compared with those of carbides. A boron substitutional effect on the carbon site in the Nb$_2$SC MAX phase was studied by Hadi et al.[35] Substitution of C and N in place of the B site of the first synthesized MAX boride Nb$_2$SB has also been reported.[42] Physical properties of predicted MAX phase borides Hf$_2$AB (A = Pb, Bi) have been reported by Hossain et al.[37] Only one MAX phase boride belonging to the 413 subclass has been investigated by Gencer[36] so far.

Miao et al.[8] have predicted MAX phase borides Hf$_2$AB (A = Bi, Pb), where they have calculated the formation energy and investigated their dynamical stability. Miao et al.[8] have also predicted another class of MAX phase materials crystallizing with different space groups (S.G.: 187, also called sub-space group of conventional MAX phase[8,45]) of the hexagonal system. The traditional MAX phases are crystallized in the S.G.: 194 of the hexagonal system. A study[8] of predicted six 212 [Ti$_2$InB$_2$, Hf$_2$AB$_2$ (In, Sn), Zr$_2$AB$_2$ (A = In, Tl, Pb)] MAX phases and two 314 [Hf$_3$PB$_4$, Zr$_3$CdB$_4$] MAX phases has been reported; among which, Ti$_2$InB$_2$ (No. 187) has already been synthesized.[45] Miao et al.[8] were inspired by the discovery of Ti$_2$InB$_2$[45] and other layered ternary borides known as the MAB phases have been investigated[46−48] in recent times. Although the B containing 212 and 314 MAX phases have layered structures that crystallize in a hexagonal system, the atomic arrangement in the cell is different from the conventional MAX phases, as shown in Figure 1. As is
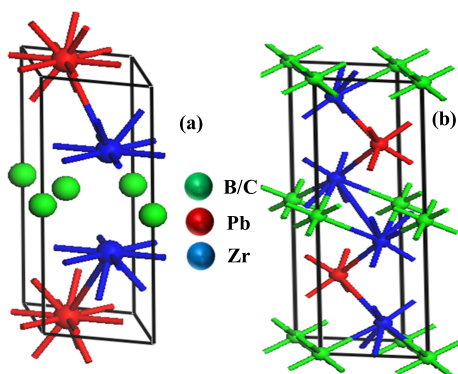

Figure 1. Unit cells of (a) Zr$_2$PbB$_2$ and (b) Zr$_2$PbB/Zr$_2$PbC MAX compounds.

evident from the figure, a 2D layer of B is sandwiched between two Zr layers that significantly contribute to the enhancement of the structural stability and mechanical strength.[49]

Li et al.[50] also predicted some MAX phase borides consisting of 212 Nb$_2$AB$_2$ [A = P, S] and 211 Nb$_2$AB [A = P, S]. Li et al.[50] have also compared their electronic and transport properties (e.g., the thermal conductivity) with 211 carbides Nb$_2$AC [A = P, S]. The stability of these phases was reported in terms of formation energy and dynamical stability. These compounds are predicted to possess unusual thermal properties owing to their acoustic and optical contributions and their anisotropic nature.

Motivated by the study of Miao et al.[8] and Li et al.,[50] we have tried to explore the 212 Ti$_2$PB$_2$ and 211 Ti$_2$PB MAX phase borides by the substitutional method. To do this, we first created

the structure of Nb$_2$PB$_2$ and Nb$_2$PB and calculated their physical properties. After then, we substituted the Nb atoms with Ti in both cases. Recently, the substitutional method has also been used by researchers to predict MAX phase borides.[36,39] Finally, we calculated their formation energy and checked their dynamical and elastic stability.

So far, the physical properties of Ti$_2$InB$_2$,[51,52] Hf$_2$AB$_2$ (A = In, Sn),[53] Zr$_2$AB$_2$ (A = In, Tl),[49] Hf$_3$PB$_4$,[54] and Zr$_3$CdB$_4$[55] MAX phases have been studied using the density functional theory (DFT) method. For each case, the mechanical properties of B-containing compounds are enhanced remarkably in comparison with their conventional C/N containing 211 MAX phases. The Debye temperature and melting temperature increased for boron-containing 212 phases compared to 211 carbides/nitrides, and the minimum thermal conductivity also decreases. The thermal expansion coefficient remains reasonably suitable for coating materials in borides. Thus, the enhanced thermomechanical properties of B-containing 212 MAX phases revealed their appropriateness for applications in high-temperature technology compared to the widely used 211 MAX phase carbides. These features of 212 MAX phases are very much motivational, and we are interested in studying the yet-to-be-investigated stable 212 MAX phase Zr$_2$PbB$_2$. Though Li et al.[50] studied transport properties, electronic band structure, Fermi surface, etc. of Nb$_2$AB$_2$ [A = P, S] and Nb$_2$AB, the mechanical properties and other thermal parameters such as Debye temperature, melting temperature, etc. are not included in their study. Moreover, we have found that Ti$_2$PB$_2$ (212) and Ti$_2$PB (211) MAX borides are energetically, elastically/mechanically, and dynamically stable.

Therefore, in this study, the thermomechanical parameters of Ti$_2$PB$_2$, Zr$_2$PbB$_2$, and Nb$_2$AB$_2$ [A = P, S] compounds have been studied employing the DFT method, and the properties are compared with those of other 212 MAX phases as well as with their 211 counterpart carbides (Ti$_2$PC, Zr$_2$PbC, Nb$_2$AC [A = P, S]) and borides (Ti$_2$PB, Zr$_2$PbB, Nb$_2$AB [A = P, S]). It is noted that the 211 boride, Zr$_2$PdB, has also been predicted in this study following the same procedure mentioned above.

2. COMPUTATIONAL METHODOLOGY

In this study, the physical properties of Ti$_2$PB$_2$, Zr$_2$PbB$_2$, and Nb$_2$AB$_2$ [A = P, S] have been computed by the Cambridge Serial Total Energy Package (CASTEP) code[56,57] via the plane-wave pseudopotential-based DFT method. The generalized gradient approximation (GGA) of the Perdew−Burke−Ernzerhof (PBE)[58] was used to treat the exchange and correlation functions. The electronic orbitals for B 2s^{2}2p^1, Pb 6s^{2}6p^2, and Zr 5s^{2}4p^{6}4d^2 were considered for pseudo-atomic calculations. The cutoff energy and k-point grids[59] were set to 500 eV and 10 × 10 × 4. The geometry was relaxed by Broyden−Fletcher−Goldfarb−Shanno's (BFGS) technique,[60] whereas density mixing was selected for the electronic structure calculations. Furthermore, the self-consistent convergence of the total energy was set to 5 × 10^{-6} eV/atom, and the maximum force per atom was taken as 0.01 eV/Å. Values of 5 × 10^{-4} Å and 0.02 GPa were fixed for the maximum ionic displacement and maximum stress. The bulk modulus (B) and shear modulus (G) were computed using Hill's approximation,[61,62] which is the average value of the upper limit (Voigt[63]) and lower limit (Reuss[64]) of B: [B = (B$_V$ + B$_R$)/2] and G: [G = (G$_V$ + G$_R$)/2]. The B$_V$, B$_R$, G$_V$, and G$_R$ can be expressed as follows:

$$B_V = \frac{1}{9}[2(C_{11} + C_{12}) + C_{33} + 4C_{13}];$$

$$B_R = \frac{(C_{11} + C_{12})C_{33} - 2C_{13}^2}{C_{11} + C_{12} + 2C_{33} - 4C_{13}};$$

$$G_V = \frac{1}{15}\{2C_{11} - C_{12} + C_{33} - 2C_{13}\}$$
$$+ \frac{1}{5}\left\{2C_{44} + \frac{1}{2}(C_{11} - C_{12})\right\};$$

and

$$G_R = \frac{5}{2}\left\{\frac{[[(C_{11} + C_{12})C_{33} - 2C_{13}^2]C_{44}C_{66}]}{[3B_V C_{44}C_{66}[(C_{11} + C_{12})C_{33} - 2C_{13}^2](C_{44} + C_{66})]}\right\};$$

$$C_{66} = (C_{11} - C_{12})/2$$

Young's modulus (Y) has been estimated using the equation $Y = 9BG/(3B + G)$.[65,66] The equation $v = (3B - Y)/(6B)$[65,66] was used to compute Poisson's ratio (v). The Cauchy pressure (CP) is obtained from the stiffness constants, $CP = (C_{12} - C_{44})$.

3. RESULTS AND DISCUSSION

3.1. Structural Properties and Stability. The structure of the conventional MAX phase is well known, but the structure of the B-containing 212 MAX phase is less familiar. The unit cell of both 212 (Zr2PbB2) and 211 (Zr2PbC) phases is presented as a representative in Figure 1 to understand the difference between the structures. As seen, there is a clear difference in the atomic arrangements in these structures, which is responsible for the different physical behaviors concerning mechanical, electronic, and thermal properties. Both 212 (Zr_2PbB_2) and 211 (Zr_2PbB/Zr_2PbC) are crystallized in the hexagonal system with different space groups. The 212 MAX phase belongs to the space group $P\bar{6}m2$ (No. 187)[8] while the 211 MAX phase belongs to the space group $P6_3/mmc$ (194).[5] The positions of M, A, and X atoms differ in the 212 and 211 MAX phases. The M (Zr) atoms are positioned at (1/3, 2/3, z_M) in the 211 phase, whereas it is at (0.3333, 0.6667, 0.6935) in the 212 phase. The atomic positions of A (Pb) atoms are at (1/3, 2/3, 3/4) and at (0.6667, 0.3333, 0.0), respectively, for the 211 and 212 phases. The most important difference is the positions and contribution of the X atoms in the bulk crystals. The X (C) atoms occupy the corner position (0, 0, 0) in the 211 phase while it (B) occupies two positions: (0.6667, 0.3333, 0.5) and (0.0, 0.0, 0.5) forming a 2D layer sandwiched in between the M layers. Within this 2D layer, the B atoms make a strong covalent bond (B−B) that results in a comparatively more stable structure than the counterpart 211 MAX phase borides and carbides.

The unit cells of Ti_2PB_2, Zr_2PbB_2, and Nb_2AB_2 [A = P, S] are optimized to obtain the other physical properties. The cell constants calculated for the optimized structures are given in Table 1. A very good consistency is observed between the values obtained in this study and prior results,[8,50] and this reveals the precision of the parameters used for calculations in this work. The lattice constants of 211 borides are presented in Table S1 (in the supplementary document).

Miao et al.[8] have shown that the predicted 212 phases including, Zr_2PbB_2, are thermodynamically stable by calculating the enthalpy with respect to the known competing phases. They have also calculated the phonon dispersion curves in which no imaginary frequency branch exists. In the case of Nb_2AB_2 [A = P, S], Li et al.[50] have shown their stability in terms of formation

Table 1. Lattice Constants (a and c) and c/a Ratio of Ti_2PB_2, Zr_2PbB_2, and Nb_2AB_2 [A = P, S] MAX Phases

phase	a (Å)	% of deviation	c (Å)	% of deviation	c/a	reference
Ti_2PB_2	3.1218		6.5457		2.09	this work
Zr_2PdB_2	3.2787	0.08	8.4282	0.15	2.57	this work
	3.276		8.415		2.57	ref[8]
Nb_2PB_2	3.1929	0.53	6.6517	0.42	2.08	this work
	3.21		6.68		2.08	ref[50]
Nb_2SB_2	3.2025	0.54	6.6548	0.52	2.07	this work
	3.22		6.69		2.07	ref[50]

energy and phonon dispersion curves. Ti_2PB_2 has been found to be stable because of the negative formation energy, non-existence of the imaginary frequency in the phonon dispersion curves, and fulfillment of the mechanical stability conditions by the calculated C_{ij}s. We have also calculated the phonon dispersion curve of Zr_2PbB_2 and Nb_2AB_2 [A = P, S] in this study, wherein no imaginary frequency branch exists, as shown in Figure 2a−d. This confirms the dynamical stability of these borides like the other 212 MAX phase borides. The phonon dispersion of corresponding 211 borides is also presented in Figure S1 (in the supplementary document).

Moreover, the mechanical stabilities of Ti_2PB_2, Zr_2PbB_2, and Nb_2AB_2 [A = P, S] have also been checked in the following section. It is noted that the formation energy of Ti_2PB_2 is calculated from the well-known formula used for the prediction of MAX phase materials:[67−72] $E_{form} = \frac{[E_{MAX} - n_M E_M - n_A E_A - n_X E_X]}{n_M + n_A + n_X}$. In this case, we have calculated the energy of all the structures of the elements found in the materials projects [tabulated in Table S2] and computed the formation energy for different combinations. The calculated values of E_{form} are found to be in the range from −1.03 to −2.38 eV/atom. Thus, it is expected that the predicted Ti_2PB_2 will be chemically stable.

3.1.1. Mechanical Properties. To bring out the figure of merit of the 212 MAX phases in light, discussing the possible relevant parameters for disclosing the mechanical properties is necessary. During the practical use of materials, many of them are subjected to applied forces or loads. Thus, knowledge of the related parameters is essential for the proper selection of the materials; otherwise, crack formation, mechanical failure, fracture introduction, or structural deformation may take place. One of the key applications of the MAX phases is as structural components at high temperatures.[73] The constants used to unveil the mechanical behavior of solids are stiffness constants, tensile strength, elastic moduli, hardness, brittleness/ductility, fracture toughness, etc. Thus, the aforementioned parameters of Ti_2PB_2, Zr_2PbB_2, and Nb_2AB_2 [A = P, S] have been estimated and discussed [Table 2]. The first step in the study of mechanical properties is the calculation of single-crystal elastic constants from which all the other mechanical parameters can be calculated. The obtained single crystal elastic constants of the titled borides using the strain−stress method[51,65,74−76] are tabulated in Table 2 along with those of previously reported 212 MAX phases and their corresponding 211 borides and/or carbides phases. The study of mechanical stability is one of the ways to assess the stability of solids under static stress used in practical applications. For this case, the stabilities of Ti_2PB_2, Zr_2PbB_2, and Nb_2AB_2 [A = P, S] are checked by the well-known stability conditions[77,78] for the hexagonal system as follows: $C_{11} > 0$, $C_{11} > C_{12}$, $C_{44} > 0$, $(C_{11} + C_{12})C_{33} - 2(C_{13})^2 > 0$. The titled
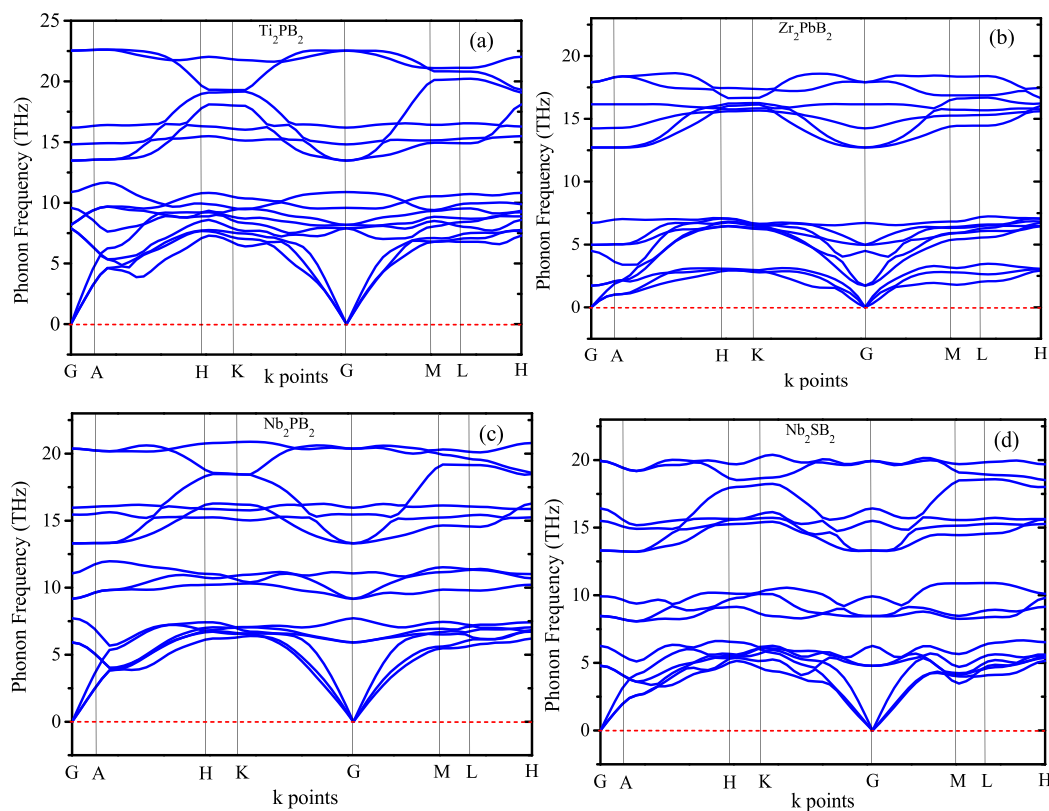
Figure 2. (a−d) Phonon dispersion curves of Ti_2PB_2, Zr_2PbB_2, and Nb_2AB_2 [A = P, S].

Table 2. Stiffness Constants, C_{ij} (GPa), Elastic Moduli [B, G, Y] (GPa), Hardness Parameters, Pugh Ratios, G/B, Poisson Ratios, ν, and Cauchy Pressures, CP (GPa) of M_2AB_2 (M = Ti, Zr, Hf, Nb; A = P, S, In, Sn, Tl, Pb) together with those of M_2AX (M = Ti, Zr, Hf, Nb; A = P, S, In, Sn, Tl, Pb; X = C, B) Compounds

phase	C_{11}	C_{12}	C_{13}	C_{33}	C_{44}	B	G	Y	H_{Chen}	H_{Miao}	G/B	ν	CP	reference
Ti_2PB_2	368	90	121	383	184	198	152	361	24.74	30.79	0.77	0.19	−94	this study
Ti_2PB	261	85	105	320	148	158	110	267	17.48	20.65	0.70	0.21	−63	this study
Ti_2PC	277	119	131	364	171	184	113	282	14.96	19.24	0.61	0.24	−52	this study
Zr_2PbB_2	297	57	72	245	76	138	95	232	15.55	17.73	0.69	0.22	−19	this study
Zr_2PbB	201	56	48	177	58	98	66	162	11.61	12.12	0.67	0.22	−02	this study
Zr_2PbC	220	66	65	216	80	116	78	191	13.08	14.28	0.67	0.23	−14	this study
Nb_2PB_2	438	115	147	476	213	241	179	430	26.36	35.49	0.74	0.20	−98	this study
Nb_2PB	350	107	141	395	199	207	146	355	21.53	27.82	0.71	0.21	−92	this study
Nb_2PC	368	123	162	400	194	225	144	355	18.72	25.24	0.64	0.23	−71	this study
Nb_2SB_2	335	90	131	404	155	196	133	326	19.20	24.58	0.68	0.22	−65	this study
Nb_2SB	326	86	126	328	151	186	128	312	19.07	23.86	0.69	0.22	−65	ref[41]
Nb_2SC	316	108	151	325	124	192	105	267	12.02	16.22	0.55	0.27	−16	ref[41]
Zr_2InB_2	315	46	64	263	82	138	105	251	19.11	21.24	0.76	0.20	−36	ref[49]
Zr_2InC	286	62	71	248	83	136	95	231	15.87	17.94	0.70	0.22	−14	ref[89]
Zr_2TlB_2	310	52	61	251	66	135	94	229	15.68	17.71	0.70	0.22	−21	ref[49]
Zr_2TlC	255	60	52	207	63	115	80	195	13.98	15.06	0.70	0.22	−03	ref[90]
Hf_2InB_2	343	61	76	278	94	154	114	274	19.46	22.56	0.74	0.20	−33	ref[53]
Hf_2InC	309	81	80	273	98	152	105	256	16.75	19.65	0.69	0.21	−17	ref[89]
Hf_2SnB_2	353	65	86	306	110	165	124	297	21.02	24.84	0.75	0.20	−45	ref[53]
Hf_2SnC	251	71	107	238	101	145	87	218	12.00	14.50	0.60	0.25	−30	ref[91]
Ti_2InB_2	364	47	58	275	94	147	122	287	23.72	26.44	0.83	0.17	−47	ref[53]
Ti_2InC	284	62	51	242	87	126	100	236	19.57	20.92	0.79	0.18	−25	ref[52]

borides satisfy the above-stated conditions, and hence they are predicted to be mechanically stable.

As can be seen in Table 2, the C_{11} and C_{33} values are not only higher for Ti_2PB_2, Zr_2PbB_2, and Nb_2AB_2 [A = P, S] compared to those of the corresponding 211 boride and carbide phases but

also higher for other 212 phases compared to their 211 counterpart carbides. In the case of C_{11}, the values are 41(33)%, 35(47)%, 25(19)%, and 12(16)% higher for Ti_2PB_2, Zr_2PbB_2, and Nb_2AB_2 [A = P, S], respectively, than that of the counterpart borides (carbides). In addition, increases of 10%, 22%, 11%,

40%, and 28% are also observed from the previously reported phases: Zr_2InB_2, Zr_2TlB_2, Hf_2InB_2, Hf_2SnB_2, Ti_2InB_2, respectively, compared to their corresponding 211 counterparts. Similarly, in the case of C_{33}, the values are 20(5)%, 38(13)%, 20(19)%, and 23(24)% for Ti_2PB_2, Zr_2PbB_2, and Nb_2AB_2 [A = P, S], respectively, than that of counterpart borides (carbides). Additionally, increases of 6%, 21%, 2%, 22%, and 14% are noted for Zr_2InB_2, Zr_2TlB_2, Hf_2InB_2, Hf_2SnB_2, and Ti_2InB_2, respectively, compared to their corresponding 211 phases. It is well known that the C_{11} and C_{33} measure bonding strength along the a and c axes. Thus, an increase of C_{11} and C_{33} implies the increase of bonding strength along the mentioned directions; consequently, the overall bonding strength is expected to be increased for 212 phases, which is also reflected in the values of elastic moduli and hardness values presented in Table 2. As we know, the bulk modulus (B) measures the resistance against uniform volume-changing hydrostatic pressure, whereas the shear modulus (G) measures the resistance against shape-changing plastic deformation. Comparative stiffness analysis of the solids can be done from the values of Young's modulus (Y), which give a measure of the resistance against change in the length. In the case of B, the values are found to be increased by 25(8)%, 41(19)%, 16(07)%, and 5(2)% for Ti_2PB_2, Zr_2PbB_2, and Nb_2AB_2 [A = P, S], respectively, compared to their counterpart borides and carbides. Similarly, shear moduli are observed to be increased by 38(34)%, 44(22)%, 23(24)%, and 4(26)%; and Young's moduli are noted to be increased by 35(28)%, 43(21)%, 21(21)%, and 4(22)% for Ti_2PB_2, Zr_2PbB_2, and Nb_2AB_2 [A = P, S], respectively, compared to their counterpart borides and carbides. Moreover, for Zr_2PbB_2, Zr_2InB_2, Zr_2TlB_2, Hf_2InB_2, Hf_2SnB_2, and Ti_2InB_2 phases, the values of $B[G(Y)]$ are increased by 1%[11%(9%)], 17%[18%(17%)], 1%[9%(7%)], 14%[43%(36%)], and 17%[22%(22%)] compared to their corresponding 211 phases Zr_2InC, Zr_2TlC, Hf_2InC, Hf_2SnC, and Ti_2InC, respectively. For 212 MAX phases, no comparison with those experimental results is possible due to the unavailability of the results. However, the elastic moduli of 211 phases can be compared with those of experimental values of the other 211 phases. For example, the values of B are 158 (184), 98 (116), 207 (225), and 186 (192) GPa for Ti_2PB (Ti_2PC), Zr_2PbB (Zr_2PbC), Nb_2PB (Nb_2PC), and Nb_2SB (Nb_2SC), respectively. The experimentally measured B values of some Ti-based 211 phases are 186 GPa (Ti_2AlC), 191 ±3 GPa (Ti_2SC), and 152 ± 3 GPa (Ti_2SnC).[79] The measured B values of some Nb-based 211 phases are 208 GPa (Nb_2AlC), 180 GPa (Nb_2SnC), and 224 ±2 GPa (Nb_2AsC).[79] Similarly, the B values of Zr-based 211 phases (Zr_2SC, 186 GPa) are also comparable.[79] Thus, the calculated values of the selected 211 borides (carbides) are comparable with those of other reported experimental values, which also indicate the reliability of our present calculations. Table 2 lists the elastic constants and elastic moduli of known 212 MAX phases. No experimental data is available for comparison. However, the elastic moduli of 212 MAX phases can be compared with those of 212 MAB phases. The $B[G(Y)]$ values of Cr_2AlB_2, Mn_2AlB_2, Fe_2AlB_2, Co_2AlB_2, and Ni_2AlB_2 are 259[197(472)], 256[165(407)], 232[139(347)], 241[101(265)], and 216[92(242)].[80] The elastic moduli of 212 MAB phases are higher than those of 212 MAX phases. The 212 MAX phases belong to the hexagonal system, while the 212 MAB phases belong to the orthorhombic system. The compositions are also different. The different crystal structures

and compositions are mainly responsible for the difference in the values of the elastic constants and moduli.

Now, we focus our attention on the hardness parameters, H_{Chen} and H_{Miao}, as calculated using the following equations: $H_{Chen} = 2[\left(\frac{G}{B}\right)^2 G]^{0.585} - 3$ [81] and $H_{Miao} = \frac{(1-2\nu)E}{6(1+\nu)}$ [82] The calculated values are presented in Table 2. As seen in Table 2, the hardness values are quite high for the studied phases. For example, the measured value of the Vickers hardness for Nb_2SB is 11.8 ± 0.37,[83] which is much lower than that of H_{Chen} (19.11 GPa) and H_{Miao} (23.86 GPa). It is well known that there is a significant difference in the measured values of hardness obtained by different methods; the calculated hardness values also differ for different formalisms. Actually, in the present case, the formulae (H_{Chen} [81] and H_{Miao} [82]) are used for the comparative prediction of the variation of hardness in between 212 and 211 MAX phases in association with their elastic moduli. To our knowledge, no experimental data for 212 MAX phases is present for comparison; we can compare the Vickers hardness of the studied 212 MAX phases with that of the measured value (10.24 ± 0.24 GPa) of 212 MAB (crystallized in orthorhombic system), Fe_2AlB_2,[84,85] and the hardness of Fe_2AlB_2 (16.86 GPa)[86] is also calculated by Chen's formula.[81] Li et al.[87] also calculated the Vickers hardness of Cr_2AlB_2 (29.6 GPa) using Chen's[81] formula, which is in line with the values of titled compounds. The different crystal structures and compositions are also responsible for the difference in the values of the Vickers hardness.

Like the elastic moduli, the hardness parameters of 212 MAX phase borides are also higher than those of 211 MAX phase borides and/or carbides. Moreover, the increase of hardness parameters is also significantly larger for Ti_2PB_2, Zr_2PbB_2, and Nb_2PB_2, while it is small for Nb_2SB_2. Increments of 20%(18%), 12%(18%), 16%(15%), 75%(71%), and 21%(26%) for H_{Chen} (H_{Miao}) are also reported in the cases of Zr_2AB_2 (A = In, Tl), Hf_2AB_2 (A = In, Sn), and Ti_2InB_2, respectively, compared to those of their corresponding 211 MAX phase carbides. Hence, it is evident that the hardness parameters are significantly enhanced for the 212 phases in comparison with the 211 phases. As discussed so far in this section, the mechanical properties of the 212 MAX phase borides are considerably enhanced compared to their counterpart 211 MAX phase borides and/or carbides. The values of C_{44} for all the studied phases also indicate a significant enhancement as it is most closely related to the hardness of solids.[88] Thus, the reasonable question is what features bring these enhancements in the 212 systems? The possible answer is explored in Section 3.5.

3.1.2. Brittleness of Ti_2PB_2, Zr_2PbB_2, and Nb_2AB_2 [A = P, S]. Although the MAX phases are metallic, most of them exhibit brittleness like ceramics. This section uses three widely known formalisms to predict brittleness/ductility. First of all, the Pugh ratio (G/B)[92] is used to confirm the brittle character of Ti_2PB_2, Zr_2PbB_2, and Nb_2AB_2 [A = P, S] [since $G/B < 0.571$ for ductile and $G/B > 0.571$ for brittle solids]. Poisson's ratio (ν) also confirmed the brittle character of Ti_2PB_2, Zr_2PbB_2, and Nb_2AB_2 [A = P, S] as $\nu = 0.26$ is a critical value to identify the brittle and ductile materials, and ν is lower than the critical value for brittle solids, and for ductile solids, the values are higher. In addition, the value of ν also indicates the bonding nature within the solids. For example, it is typically low (0.10) for covalent solids and high (0.33) for metallic solids. For the present case, it (ν) is within the range of 0.19 to 0.23, thus expecting a mixture of covalent and metallic bonding within the Ti_2PB_2, Zr_2PbB_2, and Nb_2AB_2 [A = P, S] compounds like in other MAX phases. In fact,

it agrees well with the existence of the M−X (covalent) bonding and M−A (ionic) bonding within the MAX phase materials. Moreover, Pettifor[93] addressed the Cauchy pressure (CP) to determine the chemical bonding and ductile/brittle nature of solids. A negative value of CP certifies the covalently bonded brittle solids, whereas a positive value indicates the metallic solids. As is evident, Ti_2PB_2, Zr_2PbB_2, and Nb_2AB_2 [A = P, S] belong to the covalently bonded brittle class of solids. Though these three indicators revealed the brittleness of the titled compounds, they also exhibit some ductile characteristics. For example, they are machinable and damage-tolerant, like the conventional MAX phases and the MAB phases. For instance, MoAlB has a Pugh ratio of 0.66,[94] but its damage-tolerant behavior has also been proven.[95] Bai et al.[94] explained that the layered structure and existence of different types of bonds, of which one is weaker (e.g., metallic) than others, are responsible for this unusual behavior of MoAlB. For the present case, Figure 1 shows that the titled borides exhibit a layered structure, and Table 5 indicates that there is a significant difference in the bond lengths and bond overlap populations, resulting in differences in bonding strength among different atoms. Table 5 also shows the charge transfer from M (M = Ti, Nb, and Zr) and A (A = P, Pb, S) elements to the X (X = C/B) elements. Thus, we may expect good damage-tolerant behavior for the studied compounds, like for MoAlB.

3.1.3. Elastic Anisotropy. Complete information regarding the mechanical stability of solids in extreme conditions can be gained from the study of elastic anisotropy. Anisotropy is also related to other critical processes, such as the creation and propagation of microcracks under mechanical stress, anisotropic plastic deformation, etc. Let us look back at the crystal structure again [Figure 1]; the atomic arrangements along the $a(b)$ and c directions are completely different; consequently, the bond strengths along these directions are also different [for example, $C_{11} \neq C_{33}$]. These lead to elastic anisotropy in the layered hexagonal system.[96] The knowledge of anisotropy also provides a guideline for enhancing the mechanical stability of solids under extreme conditions by supplying direction-dependent elastic constants. Thus, studying of the anisotropic nature of elastic properties is compulsory, and we have studied the elastic anisotropy of Ti_2PB_2, Zr_2PbB_2, and Nb_2AB_2 [A = P, S] by calculating some anisotropy indices using different formalisms. The different anisotropic factors for Ti_2PB_2, Zr_2PbB_2, and Nb_2AB_2 [A = P, S] are computed from elastic constants C_{ij} using the following relations[97] and presented in Table 3:

$$A_1 = \frac{\frac{1}{6}(C_{11} + C_{12} + 2C_{33} - 4C_{13})}{C_{44}}$$

$$A_2 = \frac{2C_{44}}{C_{11} - C_{12}}$$

$$A_3 = \frac{\frac{1}{3}(C_{11} + C_{12} + 2C_{33} - 4C_{13})}{C_{11} - C_{12}}$$

The compounds Ti_2PB_2, Zr_2PbB_2, and Nb_2AB_2 [A = P, S] are anisotropic, having the non-unit (one) values of A_is because $A_i = 1$ implies the isotropic nature. The linear compressibility (k) along the a and c axes is calculated by the equation[98]

$$\frac{k_c}{k_a} = f = (C_{11} + C_{12} - 2C_{13})/(C_{33} - C_{13})$$

Table 3. Anisotropy Indices, A_1, A_2, A_3, and k_c/k_a, and Universal Anisotropy Index A^U of Ti_2PB_2, Zr_2PbB_2, and Nb_2AB_2 [A = P, S] MAX Phases along with Their Counterpart Borides and Carbides

phases	A_1	A_2	A_3	k_c/k_a	A^U
Ti_2PB_2	0.67	1.32	0.89	0.82	0.14
Ti_2PB	0.64	1.68	1.07	0.63	0.33
Ti_2PC	0.58	2.16	1.27	0.58	0.67
Zr_2PbB_2	1.22	0.63	0.77	1.21	0.45
Zr_2PbB	1.20	0.80	0.96	1.25	0.06
Zr_2PbC	0.95	1.04	0.99	1.03	0.34
Nb_2PB_2	0.72	1.32	0.95	0.79	0.11
Nb_2PB	0.57	1.64	0.94	0.69	0.34
Nb_2PC	0.55	1.58	0.87	0.70	0.34
Nb_2SB_2	0.76	1.27	0.96	0.60	0.11
Nb_2SB	0.62	1.26	0.78	0.79	0.15
Nb_2SC	0.63	1.19	0.75	0.70	0.16

The computed values of f are greater than 1 ($f = 1$ for isotropic materials) for all the phases considered herein, which certify the anisotropic nature of the titled compounds.

The universal anisotropy index A^U for Ti_2PB_2, Zr_2PbB_2, and Nb_2AB_2 [A = P, S] is estimated by the following equation:[99] $A^U = 5\frac{G_V}{G_R} + \frac{B_V}{B_R} - 6 \geq 0$, where B and G are bulk and shear moduli; V and R indicate the Voigt and Reuss values. Like other anisotropy indices, A^U values for Ti_2PB_2, Zr_2PbB_2, and Nb_2AB_2 [A = P, S] are smaller than one (1), implying the anisotropic nature of Ti_2PB_2, Zr_2PbB_2, and Nb_2AB_2 [A = P, S]. Since the polycrystalline elastic moduli are calculated from the elastic constants C_{ij}, thus, it is obvious that the anisotropic behavior will be exhibited by the moduli as well. Similar results have also been reported for some other 211, 212, and 314 MAX phases previously.[49,53,54,70,100,101]

3.2. Electronic Band Structure (EBS) and Density of States (DOS). Figure 3 illustrates the EBS of Ti_2PB_2, Zr_2PbB_2, and Nb_2AB_2 [A = P, S] borides in which the electronic paths are shown in the first Brillouin zone. The obtained EBS is similar to the metallic solids due to the overlapping of the valence and conduction bands. These characteristics of MAX phase materials exhibit a good combination of metallic and ceramic properties.[41,53,102,103]

The anisotropic characteristics of the MAX phases are expected due to their layered structure. The EBS also exhibits anisotropy along the basal plane and c direction of the crystal. The paths Γ−A, H−K, and M−L correspond to the c direction while the paths A−H, K−Γ, Γ−M, and L−H are for the basal plane.[104] It is seen that the energy dispersions along the basal plane and the c direction differ significantly, confirming the anisotropic behavior of charge-effective masses for these directions, as has been found for other MAX phase nanolaminates.[41,49,53]

Figure 4a displays the partial and total DOS of Zr_2PbB_2 as a representative. These profiles roughly exhibit the usual characteristics of MAX phase materials. The Zr-d electronic states dominantly contribute the Fermi level in association with a very small contribution from the B-p and Pb-p electronic states. The strong orbital hybridization is observed between B-p states and Zr-d states that contribute to the formation of strong covalent bonding between them, similar to other MAX phases,[12,70,100] specially matched with those of Zr_2AB_2 (A = In, Tl).[49] It is worth stating that the Fermi level of Zr_2PbB_2
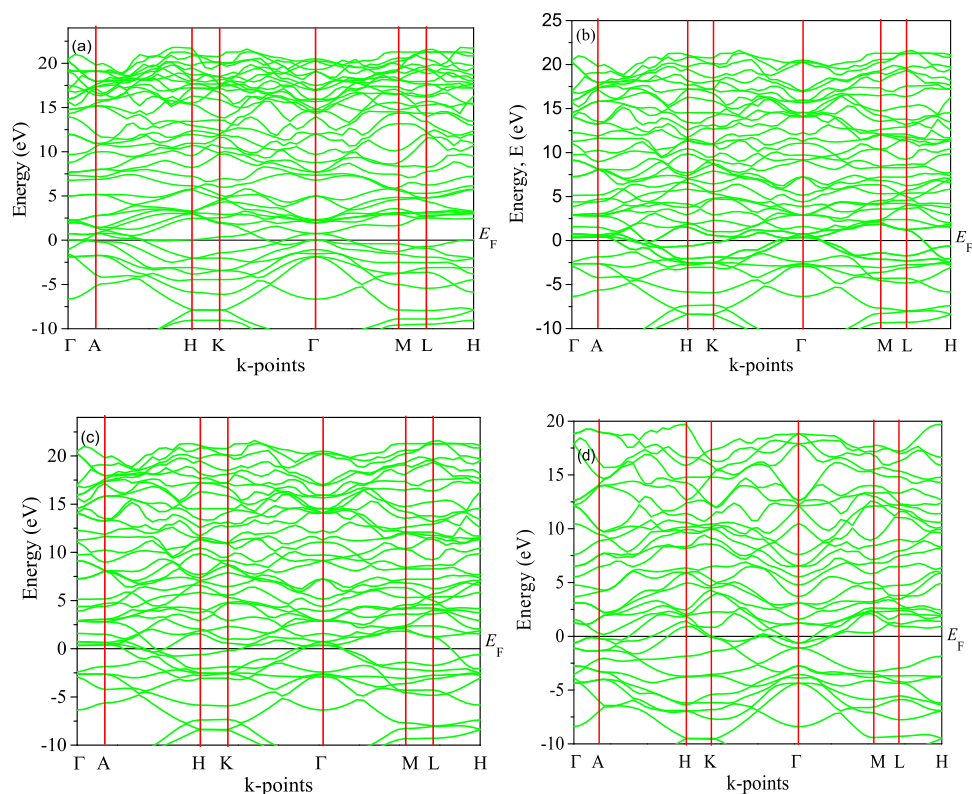
Figure 3. Electronic band structures of (a) Ti_2PB_2, (b) Zr_2PbB_2, (c) Nb_2PB_2, and (d) Nb_2SB_2 compounds.

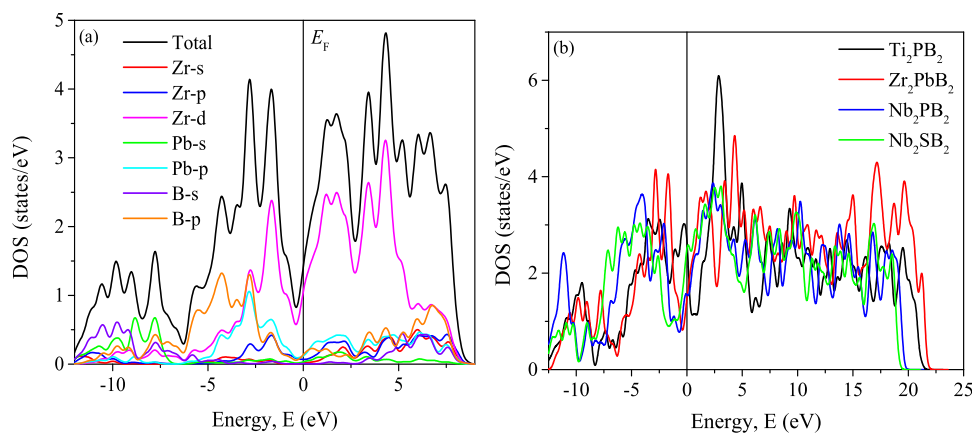**Figure 4.** Total and partial DOS of (a) Zr_2PbB_2 and (b) total DOS of Ti_2PB_2, Zr_2PbB_2, and Nb_2AB_2 [A = P, S] compounds.

resides close to the pseudogap in the TDOS profile. This is an indication of a high level of electronic stability. Similar results are also found for other compounds [not shown here]. Figure 4b shows the total DOS of the titled phases for a comparative understanding of their nature.

3.3. Thermal Properties. Recently, the high-temperature applications of MAX phases have attracted much attention from both research and application points of view. Some of the thermal parameters of particular interest can be used to assess the suitability of materials for high-temperature applications. In this section, the Debye temperature (Θ_D), minimum thermal conductivity (k_{min}), thermal expansion coefficient, Grüneisen parameter, and melting temperature of Ti_2PB_2, Zr_2PbB_2, and Nb_2AB_2 [A = P, S] compounds have been calculated to assess their potential for thermal applications.

The elastic properties can be correlated with the thermal properties; for example, phonon dynamics, thermal expansion, thermal conductivity, specific heat, and lattice enthalpy are connected to the Debye temperature. The Debye temperature itself depends on the elastic parameters that determine a material's sound velocity. The details of the calculations can be found elsewhere.[49] The obtained values of Θ_D for Ti_2PB_2, Zr_2PbB_2, and Nb_2AB_2 [A = P, S] are 861, 434, 745, and 643 K, much higher than those of the corresponding 211 borides and/or carbides [Table 4]. The Θ_D values of Ti_2PB_2 and Nb_2AB_2 [A = P, S] are also higher than those of prior known 212 phases, while Θ_D of Zr_2PbB_2 is lower than that of Zr_2InB_2, Hf_2SnB_2, and Ti_2InB_2 but greater than those of Zr_2TlB_2 and Hf_2InB_2. The Θ_D (calculated) of 212 MAB phase Fe_2AlB_2 is 750 K,[86] which is lower than that of Ti_2PB_2 (861 K) but higher than that of other 212 MAX phases presented in Table 4. On the other hand, the

Table 4. Debye Temperature, Θ_D, Minimum Thermal Conductivity, K_{min}, Grüneisen Parameter, γ, and Melting Temperature, T_m, of M_2AB_2 (M = Ti, Zr, Hf, Nb; A = P, S, In, Sn, Tl, Pb) Compounds together with those of M_2AX (M = Ti, Zr, Hf, Nb; A = P, S, In, Sn, Tl, Pb; X = C, B) Compounds

phase	ρ (g/cm³)	v_l(m/s)	v_t(m/s)	v_m(m/s)	Θ_D (K)	K_{min}(W/mK)	γ	T_m (K)	reference
Ti₂PB₂	4.45	9480	5839	6442	861	1.71	1.26	2033	this study
Ti₂PB	4.25	8460	5083	5623	704	2.43	1.35	1617	this study
Ti₂PC	4.61	8513	4947	5489	702	2.12	1.47	1731	this study
Zr₂PbB₂	8.70	5514	3304	3655	434	0.77	1.36	1613	this study
Zr₂PbB	8.25	4748	2828	3131	342	0.88	1.38	1338	this study
Zr₂PbC	9.04	4933	2937	3252	366	0.97	1.41	1223	this study
Nb₂PB₂	6.74	8435	5153	5696	745	1.45	1.29	2382	this study
Nb₂PB	6.72	7726	459	5151	635	1.80	1.34	1997	this study
Nb₂PC	6.98	7727	4541	5033	627	1.85	1.44	2058	this study
Nb₂SB₂	6.72	7449	4446	4021	643	1.39	1.37	1965	this study
Nb₂SB	6.70	7294	4366	4831	594	1.14	1.36	1824	ref[41]
Nb₂SC	6.31	7308	4079	4542	565	1.09	1.40	1790	ref[41]
Zr₂InB₂	6.87	6358	3907	4312	516	0.92	1.28	1693	ref[49]
Zr₂InC	7.32	6004	3616	3999	459	1.24	1.36	1584	ref[89]
Zr₂TlB₂	8.71	5466	3284	3633	433	0.77	1.36	1660	ref[49]
Zr₂TlC	8.92	4989	2993	3311	372	0.89	1.36	1430	ref[90]
Hf₂InB₂	10.86	5309	3240	3578	431	0.77	1.29	1800	ref[53]
Hf₂InC	11.67	5004	2999	3319	383	1.04	1.32	1691	ref[89]
Hf₂SnB₂	11.08	5459	3344	3692	447	0.80	1.28	1872	ref[53]
Hf₂SnC	12.06	5121	3050	3376	393	1.07	1.49	1746	ref[111]
Ti₂InB₂	05.90	7241	4545	5004	633	1.19	1.19	1858	ref[53]
	05.91	7168	4487	4942	621	1.23	1.20	1833	ref[52]
Ti₂InC	06.08	6531	4055	4471	534	1.00	1.23	1569	ref[52]

Θ_D values of Ti₂PB and Ti₂PC are 704 K and 702 K, which are lower than the experimental [theoretical] value of Ti₂SC (745 K [735 K]).[105] In reality, the values of Θ_D for 212 MAX phases are significantly larger than those of their B and/or C-containing counterparts belonging to the 211 MAX phases, indicating their higher temperature limits for use because the Θ_D limits the normal modes of thermal vibrations within the solids. We can quantify the degree of the increment of Debye temperature as 22.3(22.6)%, 26.3(18.6)%, 17.3(18.8)%, and 8.2(13.8)% for Ti₂PB₂, Zr₂PbB₂, and Nb₂AB₂ [A = P, S], respectively, compared to their 211 borides (carbides). The ranking of the so far known 212 MAX phases based on the values of Θ_D should be as follows: Ti₂PB₂ > Nb₂PB₂ > Nb₂SB₂ > Ti₂InB₂ > Zr₂InB₂ > Hf₂SnB₂ > Zr₂PbB₂ > Zr₂TlB₂ > Hf₂InB₂.

For the assessment of high-temperature applications, minimum thermal conductivity (k_{min}) is one of the important parameters. The thermal conductivity attains a constant value (minimum) at high temperatures, known as the minimum thermal conductivity.[106] The lower the value of k_{min}, the more suitable the solid for use in thermal barrier coating applications as it conducts less heat, which is one of the main criteria for selecting TBC materials. The k_{min} is closely associated with the acoustic wave velocity in the materials and can be calculated by the following model due to Clark:[106] $K_{min} = k_B v_m \left(\frac{M}{n \rho N_A} \right)^{-2/3}$. The values of k_{min} are significantly lower for Ti₂PB₂, Zr₂PbB₂, and Nb₂AB₂ [A = P, S] phases compared to those of the corresponding boride and carbide counterparts, as seen in Table 4. As also seen in Table 4, the K_{min} of Zr₂PbB₂ is the lowest and equal to those of Zr₂InB₂ and Hf₂InB₂, certifying a very low capability of heat conduction at high temperatures. Actually, the K_{min} of 212 phases is lower compared to their 211 counterpart borides and/or carbides, revealing more appropriateness of the 212 phases for use as TBC materials. However, we can rank

[starting from low value] the 212 phases based on the values of K_{min} as follows: Zr₂PbB₂ = Zr₂InB₂ = Hf₂InB₂ < Hf₂SnB₂ < Zr₂InB₂ < Ti₂InB₂ < Nb₂SB₂ < Nb₂PB₂ < Ti₂PB₂. The K_{min} (in the range of 0.77−1.71 W/mK) of known 212 MAX phases [Table 4] is lower than that of the 212 MAB phase, Mn₂AlB₂ (2.258 W/mK), and Fe₂AlB₂ (2.062 W/mK) calculated by Surucu et al.[107]

Owing to the close connection of the Grüneisen parameter (γ) with the specific heat at constant volume, bulk modulus, and TEC, the calculation of γ is of scientific interest. It is used to reveal the degree of anharmonic effects present in solids. Thus, γ has been determined via the relation with Poisson's ratio:[108] $\gamma = \frac{3}{2} \frac{(1 + \nu)}{(2 - 3\nu)}$. As seen, the anharmonic effect is low for Ti₂PB₂, Zr₂PbB₂, and Nb₂AB₂ [A = P, S]. The values remain within the predicted limit [0.85 to 3.53] for polycrystalline solids associated with the limiting value of Poisson's ratio [0.05−0.46].[109]

One of the mandatory information for selecting materials for applications at high-temperature technology is the melting point (T_m), which provides an idea of the temperature limit for usage. Owing to the combined ceramic properties of MAX phases with metallic properties, they have been recognized as suitable systems for high-temperature applications since the early days. Hence, the calculation of T_m for the MAX phase is essential and has been estimated in this study using the equation relating elastic constants as follows:[110] $T_m = (3C_{11} + 1.5C_{33} + 354)$ K.

Like the other 212 MAX phases, the T_m values of Ti₂PB₂, Zr₂PbB₂, and Nb₂AB₂ [A = P, S] values are also larger than their 211 corresponding counterpart borides and/or carbides. On the other hand, T_m is the lowest [1613 K] for Zr₂PbB₂ in comparison with other 212 MAX phase borides, while it is maximum for Nb₂PB₂ [2382 K] (Table 4). In addition, the formula used to calculate the T_m contains C_{11} and C_{33}, which are

the measures of the stiffness along the a and c axes. Thus, a direct relationship between the T_m and Young's modulus [a measure of the stiffness of a polycrystalline solid] is expected, which is seen in Tables 2 and 4. The maximum value of Y is obtained for Nb_2PB_2, following the ranking $Nb_2PB_2 > Ti_2PB_2 > Nb_2SB_2 > Hf_2SnB_2 > Ti_2InB_2 > Hf_2InB_2 > Zr_2InB_2 > Zr_2TlB_2 > Zr_2PbB_2$. This ranking also applies to the melting temperature T_m as seen in Table 4. It has been suggested previously that T_m will be higher for the solids with higher Young's modulus and vice versa.[112] Knowledge regarding the decomposition temperature (T_d) is also a prerequisite regardless of the value of T_m. The MAX phases have a tendency to decompose at a lower temperature than that of T_m. Unfortunately, no information regarding the T_d of the titled borides as well as the other 212 phases is present at this moment. An earlier report provided by Cui et al.[113] might be helpful regarding this issue. They have estimated T_d and T_m of some MAX phases and shown that T_d is lower than T_m; for some cases, T_d is close to T_m;[54] thus, one may expect the same for Ti_2PB_2, Zr_2PbB_2, and Nb_2AB_2 [A = P, S] phases as well.

3.4. Why are the Thermomechanical Properties for 212 Phases Enhanced? From the analysis of the results obtained so far, it is obvious that the thermomechanical properties are significantly upgraded when we go from the 211 MAX phase carbides to the 212 MAX phase borides. Why are the properties enhanced for the 212 phases? The answer lies in the structure. Though both the 212 and 211 phases belong to the MAX family, their structures are not the same. The 212 phases are crystallized in the space group $P-6m2$, (No. 187),[8,45] while the 211 phases are crystallized in the space group $P6_3/mmc$ (No.194)[5,114] as shown in Figure 1a,b. The bonding natures within these two structures are also different. For the 212 phases, there is a very strong covalent bonding among the B atoms by forming a 2D layer and contributing to the 2c-2e type of bonding, as shown in Figure 5a,b. In addition, there is also strong
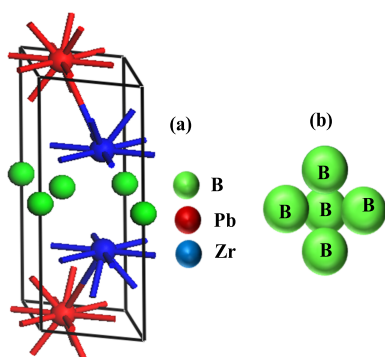

Figure 5. Unit cell of Zr_2PbB_2 (a) and formation of the B−B covalent bonding (b) within Zr_2PbB_2.

covalent bonding between M (Zr atoms for Zr_2PbB_2) and X (B atoms for Zr_2PbB_2) similar to the 211 phases (Zr and B/C are M and X atoms for Zr_2PbB/Zr_2PbC). In addition, there is comparatively weak M−A bonding (Pb is the A atom in the case of Zr_2PbB/Zr_2PbC). There is no covalent bond among the C atoms in the 211 phase, although strong covalent bonds between M−X atoms and the M−A bonds are formed. The structure becomes more stable due to the existence of the very strong B−-B covalent bonding within the 2D layer of B atoms, and the overall cohesive energy is enhanced significantly for the 212 phases in comparison with the 211 phases. It is noted that,

for 211 MAX phase borides, B−B bonding does not exist.[6,7,35,37,41,115] Our statements will be further clarified by the calculation of the Mulliken population analysis given in Table 5. As seen in Table 5, the charge is transferred from Zr to B (0.54/0.55) and Pb (0.01). The charge transfer mechanism confirms the existence of an ionic character as observed for the B/C-containing MAX phase Zr_2PbB/Zr_2PbC. In this boride/carbide, the charge is transferred from Zr to B (0.77) and Pb (0.00) [Table 5]. Table 5 also shows the bond overlap population (BOP) analysis for both the compounds Zr_2PbB_2 and Zr_2PbB. The value of BOP indicates the nature of bonding/anti-bonding states within the solids depending on the positive/negative values. A negative value of BOP stands for anti-bonding, whereas a positive value is for bonding states. It is clear from Table 5 that no anti-bonding exists within the considered MAX phases. In addition, the value of BOP is also an indicator of bonding strength; the higher the BOP, the stronger the bonding. As is evident from Table 5, the B−B bonding exhibits a much higher BOP value, confirming the very strong covalent bonding formed in the 2c-2e channel. The M (Zr)−X (B) bonding in Zr_2PbB is stronger than that of Zr_2PbB_2 with BOP values of 1.25 and 0.24/0.20, respectively. Due to very strong B−B bonding, the overall bonding strength, mechanical parameters, and hardness values are higher for Zr_2PbB_2 compared to Zr_2PbB. The results for the other titled compounds are also presented in Table 5. Similar results are also reported for other known 212 phases.[49,51,53]

Now, let us discuss the variation of the mechanical properties [Table 2] among the titled borides in terms of the BOP values as presented in Table 5. We can rank the titled borides based on the values of hardness parameters [Table 2] (H_{chen}, H_{miao}, and C_{44}) as follows: $Nb_2PB_2 > Ti_2PB_2 > Nb_2SB_2 > Zr_2PbB_2$. The BOP values of B−B bonds are 2.22, 2.47, 2.07, and 2.12 for Nb_2PB_2, Ti_2PB_2, Nb_2SB_2, and Zr_2PbB_2, respectively. According to these values, the ranking of borides can be re-ordered. However, for Nb_2PB_2, the BOPs of Nb-B are (0.14 and 0.19) higher compared to those of Ti-B (0.05 and 0.12), and the BOP of Nb-P and Ti-P is the same for both compounds. Thus, considering the cumulative contribution from all bonds (BOP), the overall bonding strength is expected to be higher for Nb_2PB_2 compared to that for Ti_2PB_2, which is reflected in values of the elastic constants, elastic moduli, and hardness parameters. Again for Nb_2SB_2 and Zr_2PbB_2, the BOPs of the B−B bond are 2.07 and 2.12, respectively. The BOPs of Nb-B (0.20 and 0.19) and Zr-B (0.24 and 0.20) are also comparable. However, there is no BOP for Zr-Pb bonding within the considered threshold length (5 Å), whereas the BOP for Nb-S is 0.74. This makes the difference in the overall bonding strength as reflected from values of elastic constants, elastic moduli, and hardness parameters. It is also noted that no BOP of Zr-Pb is found for the 211 Zr_2PbB compound [Table 5].

3.5. Optical Properties. The technologically important optical constants of Ti_2PB_2, Zr_2PbB_2, and Nb_2AB_2 [A = P, S] MAX phase compounds are estimated and shown in Figure 6 in the energy range up to 25 eV. The low energy part of the imaginary part of the dielectric function is corrected by introducing a plasma frequency of 3 eV and damping of 0.5 eV owing to the metallic nature of the titled compounds. Additionally, we have used a Gaussian smearing of 0.5 eV. The obtained optical properties are compared (distinctive values, figures are not shown) with those of the most widely studied MAX phase Ti_3SiC_2 as calculated by Li et al.[116] and those of Ti_2AlC and Ti_2AlN measured by Haddad et al.[117] The results

Table 5. Mulliken Atomic and Bond Overlap Populations of Ti_2PB_2, Zr_2PbB_2, and Nb_2AB_2 [A = P, S] and Ti_2PB, Zr_2PbB, and Nb_2AB [A = P, S] MAX Compounds

compound	atoms	atomic population					bond overlap population			
		s	p	d	total	charge (e)	bond	bond number n^μ	bond length d^μ (Å)	bond population P^μ
Ti_2PB_2	B	0.95	2.62	0.00	3.56	−0.56	B−B	1	1.80242	2.47
	B	0.95	2.61	0.00	3.57	−0.57	Ti−B	2	2.39781	0.12
	Ti	2.10	6.51	2.79	11.39	0.61	Ti−B	2	2.39781	0.05
	P	1.58	3.50	2.79	5.08	0.08	Ti−P	2	2.47181	1.00
Ti_2PB	B	1.21	2.42	0.00	3.64	−0.64	Ti−B	4	2.27017	1.10
	Ti	2.21	6.67	2.73	11.62	0.38	Ti−P	4	2.49843	0.96
	P	1.61	3.52	0.00	5.13	−0.13				
Zr_2PbB_2	B	0.98	2.58	0.00	3.55	−0.55	B−B	1	1.89298	2.12
	B	0.97	2.57	0.00	3.54	−0.54	Zr−B	2	2.51753	0.24
	Zr	2.15	6.46	2.84	11.45	0.55	Zr−B	2	2.51753	0.20
	Pb	1.42	2.55	10.04	14.01	−0.01				
Zr_2PbB	B	1.18	2.59	0.00	3.77	−0.77	Zr−B	4	2.38633	1.25
	Zr	2.28	6.61	2.72	11.62	0.38				
	Pb	1.41	2.55	10.03	14.00	00.0				
Nb_2PB_2	B	0.92	2.57	0.00	3.49	−0.49	B−B	1	1.84346	2.22
	B	0.95	2.56	0.00	3.51	−0.51	Nb−B	2	2.43378	0.19
	Nb	2.15	6.28	4.07	15.51	0.49	Nb−B	2	2.43378	0.14
	P	1.55	3.43	0.00	4.99	0.01	Nb−P	2	2.53279	1.00
Nb_2PB	B	1.14	2.46	0.00	3.60	−0.60	Nb−B	4	2.29051	1.15
	Nb	2.25	6.41	4.02	12.68	0.32	Nb−P	4	2.56130	1.06
	P	1.59	3.46	0.00	5.04	−0.04				
Nb_2SB_2	B	0.92	2.56	0.00	3.47	−0.47	B−B	1	1.84897	2.07
	B	0.93	2.58	0.00	3.51	−0.51	Nb−B	2	2.40337	0.20
	Nb	2.14	6.27	4.04	12.45	0.55	Nb−B	2	2.40337	0.19
	S	1.76	4.37	0.00	6.12	−0.12	Nb−S	2	2.57488	0.74
Nb_2SB	B	1.11	2.51	0.00	3.62	−0.62	Nb−B	4	2.26543	1.12
	S	1.77	4.40	0.00	6.17	−0.17	Nb−S	4	2.59817	0.79
	Nb	2.24	6.37	3.99	12.61	0.39				

were also compared with those of the Cr_2AlB_2 MAB compound calculated by Li et al.[87]

The real part of the dielectric function, ε_1, is shown in Figure 6a, exhibiting metallic behavior. Usually, the ε_1 exhibit a large negative value in the very low energy region for metallic systems. Haddad et al.[117] and Li et al.[116] also obtained such negative values for Ti_2AlC and Ti_2AlN and for Ti_3SiC_2. The first peak is noticed at ~1.5 eV for Ti_3SiC_2, while it is around 5 eV for both Ti_2AlC and Ti_2AlN phases. For the titled phases, the 1st peaks are obtained in the 0.5−2.5 eV range. Thus, the ε_1 spectra of Ti_2PB_2, Zr_2PbB_2, and Nb_2AB_2 [A = P, S] agree well with the non-existence of the energy band gap in the electronic band structure. The imaginary part of dielectric function ε_2 is depicted in Figure 6b, wherein two small peaks are observed for both polarization directions of the electric field vector. The peaks in the ε_2 certify that Ti_2PB_2, Zr_2PbB_2, and Nb_2AB_2 [A = P, S] compounds are metals, and the E_F [Figure 3] is located at the Ti-3d states that result in the free electron behavior; consequently, the photon-induced transition between electronic states is possible within the conduction band. The nature of ε_1 and ε_2 spectra of the studied compounds is similar to those of Ti_3SiC_2; ε_2 also started with a high value, showing some peaks in low energy sides and becoming zero (both ε_1 and ε_2); ε_1 reached zero from below while ε_2 from above. The optical properties of the Cr_2AlB_2 MAB phase have been reported by Li et al.[87] The spectra for ε_1 and ε_2 are not matched in the lower energy region with the present study; the authors did not introduce a plasma frequency during the calculation of dielectric function that is mandatory for metallic systems. In another unpublished work,[118] where the

dielectric function of Cr_2GeC, Nb_2AlC, Ti_2AlC, Ti_2AlN, Ti_2SC, and Ti_3GeC_2 was measured up to 5 eV, the low energy of the spectra matched well with the present results.

The refractive index (n) and extinction coefficient (k) are depicted in Figure 6c,d, respectively. The $n(0)$ is found to be 6.4, 7.8, 7.1, and 18.6 for Ti_2PB_2, Zr_2PbB_2, and Nb_2AB_2 [A = P, S], respectively. The k values for Ti_2PB_2, Zr_2PbB_2, and Nb_2AB_2 [A = P, S] rise progressively in the IR region to their highest values and then decline slowly in the visible and UV regions [Figure 6d]. The decline of k follows the decline of ε_2, as seen in Figure 6b,d. The variation of n and k spectra with photon energy agrees well with those of the Cr_2AlB_2 MAB phase as calculated by Li et al.;[87] the static value of the $n(0)$ is ~7.3, which is higher than that of Ti_2PB_2 and Nb_2PB_2 but lower than those of Zr_2PbB_2 and Nb_2SB_2 [A = P, S] phases.

The absorption coefficient (α) of Ti_2PB_2, Zr_2PbB_2, and Nb_2AB_2 [A = P, S] is presented in Figure 6e. As seen in the figure, it rises almost steadily to attain its maximum value in the UV region. Moreover, α starts rising from the zero photon energy, indicating once again the metallic nature of the compounds under investigation. In addition, it is found that Ti_2PB_2, Zr_2PbB_2, and Nb_2AB_2 [A = P, S] can be used as good absorbing materials in the visible and UV regions owing to the high values of their absorption coefficients. Figure 6f displays the photoconductivity (σ) of Ti_2PB_2, Zr_2PbB_2, and Nb_2AB_2 [A = P, S] as a function of photon energy. The σ measures the change in the electrical conductivity of the material when it is subjected to photon irradiation. Like α, the σ spectrum also certifies that Ti_2PB_2, Zr_2PbB_2, and Nb_2AB_2 [A = P, S] are metallic
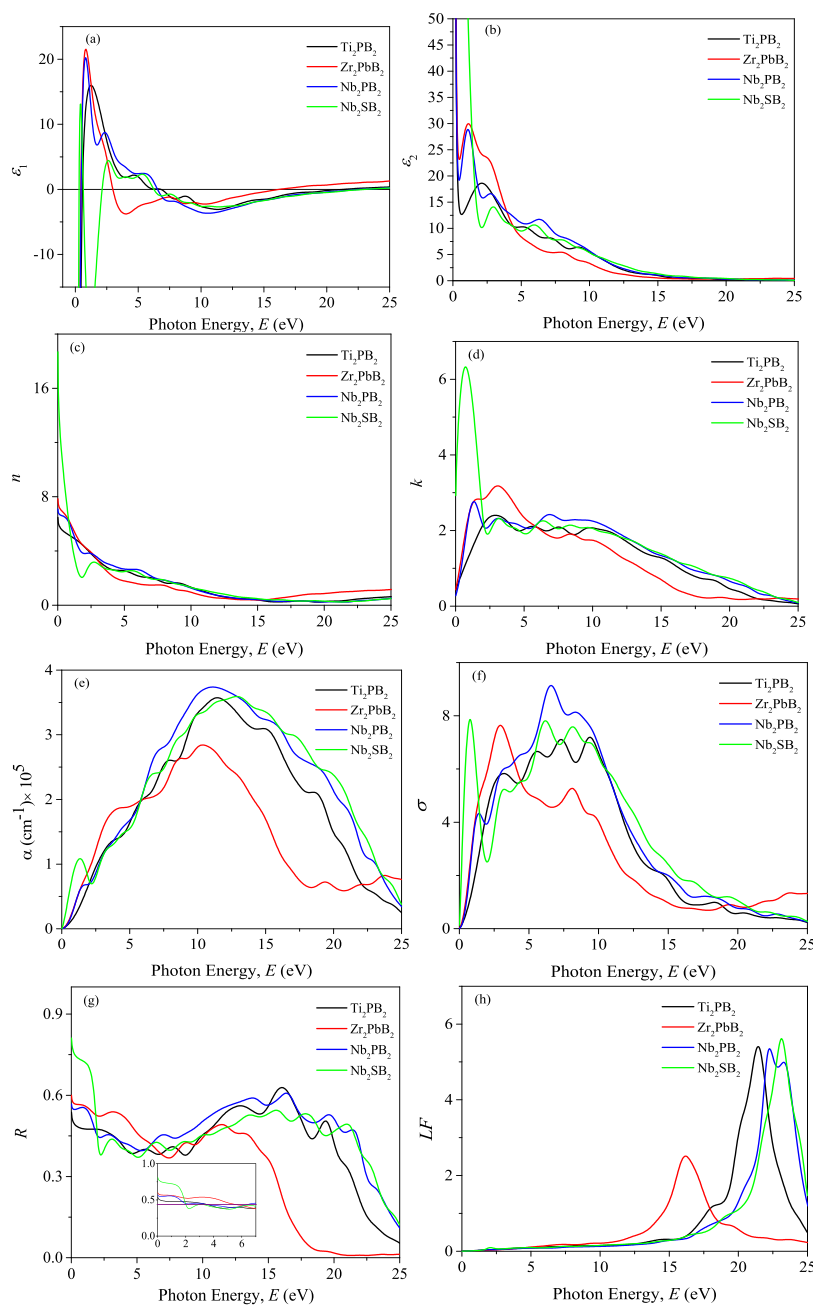
Figure 6. (a) Real part, ε_1, and (b) imaginary part of the dielectric function, ε_2, (c) refractive index, n, (d) extinction coefficient, k, (e) absorption coefficient, α, (f) photoconductivity, σ, (g) reflectivity, R, and (h) loss function, L, as a function of photon energy.

compounds. Li et al.[87] also reported similar results for Cr_2AlB_2 with a slight variation in the position and height of the peaks. For example, the strongest absorption zone is 3 to 15 eV, which is close to that of Zr_2PbB_2 and lower than that of Ti_2PB_2 and Nb_2AB_2 [A = P, S] phases.

One of the most important applications of MAX phase materials is as coating materials to reduce solar heating. The potential for this application can be predicted by the study of reflectivity. The reflectivity $R(\omega)$ of Ti_2PB_2, Zr_2PbB_2, and Nb_2AB_2 [A = P, S] is presented in Figure 6g. According to Li et al.,[116,119] the MAX phase materials, which have reflectivity greater than 44%, are suitable for use as coating materials. As is evident from Figure 6g, the $R(\omega)$ always remains greater than 44% up to ~12 eV for all the considered phases. Though the reflectivity at low energy is the highest for Nb_2SB_2, the overall

performance of Zr_2PbB_2 is the best for use as a cover to protect from solar heating. Noted here is that the reflectivity spectrum with ~53% in the IR, visible, and near UV region (0−5 eV) was almost constant for Zr_2PbB_2. The reflectivity spectrum of Ti_3SiC_2 started with a value of ~0.75, going down at around 1 eV remaining almost constant up to 6 eV.[116] On the other hand, for Cr_2AlB_2, it started with a value of 0.55, reached the lowest value (lower than 40%) at around 4 eV, and again rose to reach the maximum of 0.96 at 15.3 eV. The reflectivity of Zr_2PbB_2 is almost similar to that of Ti_3SiC_2 up to 6 eV. The overall reflective behavior of the titled borides is better than that of Cr_2AlB_2.[87] Figure 6h shows the energy loss function $[L(\omega)]$ spectra of Ti_2PB_2, Zr_2PbB_2, and Nb_2AB_2 [A = P, S] compounds, in which the peaks correspond to plasma frequencies (ω_p). At this particular frequency, the $R(\omega)$ exhibits a falling tail, the

absorption coefficient falls rapidly, and ε_1 crosses zero from the negative side. It is the characteristic frequency above which the materials behave as transparent to the incident electromagnetic wave. The ω_p values of Ti_2PB_2, Zr_2PbB_2, and Nb_2AB_2 [A = P, S] are 21.3, 16.1, 22.2, and 23.1 eV, respectively. The measured ω_p of Ti_2AlC and Ti_2AlN is around 17 eV[118], which is comparable to the present results. The nature of the loss function of Cr_2AlB_2 is similar to those in the present results, the plasma frequency (ω_p) of which is 16.0 eV[87].

4. CONCLUSIONS

The thermomechanical and optical properties of Ti_2PB_2, Zr_2PbB_2, and Nb_2AB_2 [A = P, S] are explored via DFT calculations with the intention of shedding light on the enhanced thermomechanical properties of recently added 212 MAX phase borides in comparison with their 211 boride and carbide counterparts. The titled MAX phases are chemically, dynamically, and mechanically stable. The values of elastic constants and moduli of 212 phases are higher than those of the 211 phase borides and/or carbides. The hardness parameters are also higher for 212 phases. The titled borides also exhibit the usual brittleness of the MAX phase. Due to the different atomic arrangements along the a and c directions, the elastic properties are anisotropic. The EBS and DOS confirm the metallic character of the studied phases. Like the mechanical properties, the thermal parameters are also enhanced significantly for 212 phases compared to their 211 counterparts. For Θ_D, the values are increased by 22.3(22.6)%, 26.3(18.6)%, 17.3(18.8)%, and 8.2(13.8)% for Ti_2PB_2, Zr_2PbB_2, and Nb_2AB_2 [A = P, S], respectively, compared to the corresponding 211 borides (carbides). The melting temperature is also noted to be increased by 26(17)%, 20(32)%, 19(16)%, and 08(10)%. The study of thermomechanical properties reveals the appropriateness of the 212 phase borides compared to their 211 counterpart MAX phases for applications. The existence of very strong B−B bonding contributes to the enhancement of the thermomechanical properties of the 212 compounds. The important results concerning the optical constants are found in accord with the electronic band structure results. The dielectric constant, absorption coefficient, and photoconductivity spectra reconfirm the metallic nature of the titled MAX phases. The reflectivity spectra show the suitability of Ti_2PB_2, Zr_2PbB_2, and Nb_2AB_2 [A = P, S] phases for use as shielding materials to protect from solar radiation.

To conclude, we hope the results presented in this paper will stimulate further research on the 212 MAX phases, which exhibit superior characteristics for applications in the thermomechanical sectors compared to many other conventional MAX phase nanolaminates.

ASSOCIATED CONTENT

Ⓢ Supporting Information

The Supporting Information is available free of charge at https://pubs.acs.org/doi/10.1021/acsomega.2c06331.

> Lattice parameters of Ti_2PB, Zr_2PbB, and Nb_2AB [A = P, S] MAX phase compounds (Table S1); different structures of Ti_2PB_2 composing elements (Table S2); phonon dispersion curve (Figure S1); electronic band structure (Figure S2) and DOS (Figure S3) of Ti_2PB, Zr_2PbB, and Nb_2AB [A = P, S] MAX phase compounds (PDF)

AUTHOR INFORMATION

Corresponding Authors

Md. Ashraf Ali − *Department of Physics and Advanced Computational Materials Research Laboratory (ACMRL), Department of Physics, Chittagong University of Engineering and Technology (CUET), Chattogram 4349, Bangladesh;* ⓞ orcid.org/0000-0003-4957-2192; Email: ashrafphy31@cuet.ac.bd

Saleh Hasan Naqib − *Advanced Computational Materials Research Laboratory (ACMRL), Department of Physics, Chittagong University of Engineering and Technology (CUET), Chattogram 4349, Bangladesh; Department of Physics, University of Rajshahi, Rajshahi 6205, Bangladesh;* Email: salehnaqib@yahoo.com

Authors

Md. Mukter Hossain − *Department of Physics and Advanced Computational Materials Research Laboratory (ACMRL), Department of Physics, Chittagong University of Engineering and Technology (CUET), Chattogram 4349, Bangladesh;* ⓞ orcid.org/0000-0003-2454-4996

Md. Mohi Uddin − *Department of Physics and Advanced Computational Materials Research Laboratory (ACMRL), Department of Physics, Chittagong University of Engineering and Technology (CUET), Chattogram 4349, Bangladesh*

A. K. M. Azharul Islam − *Department of Electrical and Electronic Engineering, International Islamic University Chittagong, Chattogram 4318, Bangladesh; Department of Physics, University of Rajshahi, Rajshahi 6205, Bangladesh*

Complete contact information is available at:
https://pubs.acs.org/10.1021/acsomega.2c06331

Author Contributions

M. A. Ali: Conceptualization, Methodology, Formal analysis, Validation, Project administration, Writing − original draft. **M. M. Hossain:** Methodology, Formal analysis, Writing − original draft, review & editing, Validation; **M. M. Uddin:** Writing − review & editing, Validation; **A. K. M. A. Islam:** Writing − review & editing, Validation; **S. H. Naqib:** Writing − review & editing, Validation, Supervision.

Notes

The authors declare no competing financial interest.

ACKNOWLEDGMENTS

REFERENCES

(1) Sokol, M.; Natu, V.; Kota, S.; Barsoum, M. W. On the Chemical Diversity of the MAX Phases. *Trends Chem.* **2019**, *1*, 210−223.

(2) Barsoum, M. W. Physical Properties of the MAX Phases. In *Encyclopedia of Materials: Science and Technology*; Elsevier, 2006; pp 1−11. DOI: 10.1016/B0-08-043152-6/02058-1.

(3) Barsoum, M. W.; Brodkin, D.; El-Raghy, T. Layered Machinable Ceramics for High Temperature Applications. *Scr. Mater.* **1997**, *36*, 535−541.

(4) Barsoum, M. W. The $M_{N+1}AX_N$ Phases: A New Class of Solids. *Prog. Solid State Chem.* **2000**, *28*, 201−281.

(5) Barsoum, M. W. *MAX Phases: Properties of Machinable Ternary Carbides and Nitrides*; Wiley-VCH Verlag GmbH & Co. KGaA: Weinheim, Germany, 2013. DOI: 10.1002/9783527654581.

(6) Khazaei, M.; Arai, M.; Sasaki, T.; Estili, M.; Sakka, Y. Trends in Electronic Structures and Structural Properties of MAX Phases: A First-Principles Study on M_2AlC (M = Sc, Ti, Cr, Zr, Nb, Mo, Hf, or Ta), M_2AlN, and Hypothetical M_2AlB Phases. *J. Phys. Condens. Matter* 2014, 26, 505503.

(7) Rackl, T.; Eisenburger, L.; Niklaus, R.; Johrendt, D. Syntheses and Physical Properties of the MAX Phase Boride Nb_2SB and the Solid Solutions $NB_2SB_xC_{1-x}$ (X=0-1). *Phys. Rev. Mater.* 2019, 3, No. 054001.

(8) Miao, N.; Wang, J.; Gong, Y.; Wu, J.; Niu, H.; Wang, S.; Li, K.; Oganov, A. R.; Tada, T.; Hosono, H. Computational Prediction of Boron-Based MAX Phases and MXene Derivatives. *Chem. Mater.* 2020, 32, 6947−6957.

(9) Naguib, M.; Mochalin, V. N.; Barsoum, M. W.; Gogotsi, Y. 25th Anniversary Article: MXenes: A New Family of Two-Dimensional Materials. *Adv. Mater.* 2014, 26, 992−1005.

(10) Jeitschko, W.; Nowotny, H.; Benesovsky, F. Carbides of Formula T_2MC. *J. Less Common Met.* 1964, 7, 133−138.

(11) Ali, M. A. Newly Synthesized Ta-Based MAX Phase $(Ta_{1-x}Hf_x)_4AlC_3$ and $(Ta_{1-x}Hf_x)_4Al_{0.5}Sn_{0.5}C_3$ ($0 \leq x \leq 0.25$) Solid Solutions: Unravelling the Mechanical, Electronic, and Thermodynamic Properties. *Phys. Status Solidi* 2021, 258, 2000307.

(12) Khatun, M. R.; Ali, M. A.; Parvin, F.; Islam, A. K. M. A. Elastic, Thermodynamic and Optical Behavior of V_2AC (A = Al, Ga) MAX Phases. *Results Phys.* 2017, 7, 3634−3639.

(13) Ingason, A. S.; Dahlqvist, M.; Rosen, J. Magnetic MAX Phases from Theory and Experiments A Review. *J. Phys. Condensed Matter.* 2016, No. 433003.

(14) Lapauw, T.; Lambrinou, K.; Cabioc'h, T.; Halim, J.; Lu, J.; Pesach, A.; Rivin, O.; Ozeri, O.; Caspi, E. N.; Hultman, L.; Eklund, P.; Rosén, J.; Barsoum, M. W.; Vleugels, J. Synthesis of the New MAX Phase Zr_2AlC. *J. Eur. Ceram. Soc.* 2016, 36, 1847−1853.

(15) Lapauw, T.; Halim, J.; Lu, J.; Cabioc'h, T.; Hultman, L.; Barsoum, M. W.; Lambrinou, K.; Vleugels, J. Synthesis of the Novel Zr_3AlC_2 MAX Phase. *J. Eur. Ceram. Soc.* 2016, 36, 943−947.

(16) Dahlqvist, M.; Lu, J.; Meshkian, R.; Tao, Q.; Hultman, L.; Rosen, J. Prediction and Synthesis of a Family of Atomic Laminate Phases with Kagomé-like and in-Plane Chemical Ordering. *Sci. Adv.* 2017, 3, 1−10.

(17) Fashandi, H.; Lai, C. C.; Dahlqvist, M.; Lu, J.; Rosen, J.; Hultman, L.; Greczynski, G.; Andersson, M.; Lloyd Spetz, A.; Eklund, P. Ti_2Au_2C and $Ti_3Au_2C_2$ Formed by Solid State Reaction of Gold with Ti_2AlC and Ti_3AlC_2. *Chem. Commun.* 2017, 53, 9554−9557.

(18) Mian, L.; You-Bing, L.; Kan, L.; Jun, L.; Per, E.; Per, P.; Johanna, R.; Lars, H.; Shi-Yu, D.; Zheng-Ren, H.; Qing, H. Synthesis of Novel MAX Phase Ti_3ZnC_2 via A-Site-Element-Substitution Approach. *J. Inorg. Mater.* 2019, 34, 60.

(19) Lapauw, T.; Tunca, B.; Cabioc'h, T.; Lu, J.; Persson, P. O. Å.; Lambrinou, K.; Vleugels, J. Synthesis of MAX Phases in the Hf−Al−C System. *Inorg. Chem.* 2016, 55, 10922−10927.

(20) Anasori, B.; Dahlqvist, M.; Halim, J.; Moon, E. J.; Lu, J.; Hosler, B. C.; Caspi, E. N.; May, S. J.; Hultman, L.; Eklund, P.; Rosén, J.; Barsoum, M. W. Experimental and Theoretical Characterization of Ordered MAX Phases Mo_2TiAlC_2 and $Mo_2Ti_2AlC_3$. *J. Appl. Phys.* 2015, 118, No. 094304.

(21) Kuchida, S.; Muranaka, T.; Kawashima, K.; Inoue, K.; Yoshikawa, M.; Akimitsu, J. Superconductivity in Lu_2SnC. *Phys. C* 2013, 494, 77−79.

(22) Xu, Q.; Zhou, Y.; Zhang, H.; Jiang, A.; Tao, Q.; Lu, J.; Rosén, J.; Niu, Y.; Grasso, S.; Hu, C. Theoretical Prediction, Synthesis, and Crystal Structure Determination of New MAX Phase Compound V_2SnC. *J. Adv. Ceram.* 2020, 9, 481−492.

(23) Ali, M. S.; Rayhan, M. A.; Ali, M. A.; Parvin, R.; Islam, A. K. M. A. New MAX Phase Compound Mo_2TiAlC_2: First-Principles Study. *J. Sci. Res.* 2016, 8, 109−117.

(24) Horlait, D.; Middleburgh, S. C.; Chroneos, A.; Lee, W. E. Synthesis and DFT Investigation of New Bismuth-Containing MAX Phases. *Sci. Rep.* 2016, 2016, 1−9.

(25) Zapata-Solvas, E.; Hadi, M. A.; Horlait, D.; Parfitt, D. C.; Thibaud, A.; Chroneos, A.; Lee, W. E. Synthesis and Physical Properties of $(Zr_{1-x}Ti_x)_3AlC_2$ MAX Phases. *J. Am. Ceram. Soc.* 2017, 100, 3393−3401.

(26) Naguib, M.; Bentzel, G. W.; Shah, J.; Halim, J.; Caspi, E. N.; Lu, J.; Hultman, L.; Barsoum, M. W. New Solid Solution MAX Phases: $(Ti_{0.5}V_{0.5})_3AlC_2$, $(Nb_{0.5}V_{0.5})_2AlC$, $(Nb_{0.5}V_{0.5})_4AlC_3$ and $(Nb_{0.8}Zr_{0.2})_2AlC$. *Mater. Res. Lett* 2014, 2, 233−240.

(27) Burr, P. A.; Horlait, D.; Lee, W. E. Experimental and DFT Investigation of $(Cr,Ti)_3AlC_2$ MAX Phases Stability. *Mater. Res. Lett.* 2017, 5, 144−157.

(28) Tunca, B.; Lapauw, T.; Karakulina, O. M.; Batuk, M.; Cabioc'h, T.; Hadermann, J.; Delville, R.; Lambrinou, K.; Vleugels, J. Synthesis of MAX Phases in the Zr-Ti-Al-C System. *Inorg. Chem.* 2017, 56, 3489−3498.

(29) Lapauw, T.; Tunca, B.; Potashnikov, D.; Pesach, A.; Ozeri, O.; Vleugels, J.; Lambrinou, K. The Double Solid Solution $(Zr, Nb)_2(Al, Sn)C$ MAX Phase: A Steric Stability Approach. *Sci. Rep.* 2018, 8, 12801.

(30) Tunca, B.; Lapauw, T.; Delville, R.; Neuville, D. R.; Hennet, L.; Thiaudière, D.; Ouisse, T.; Hadermann, J.; Vleugels, J.; Lambrinou, K. Synthesis and Characterization of Double Solid Solution $(Zr,Ti)_2(Al,Sn)C$ MAX Phase Ceramics. *Inorg. Chem.* 2019, 58, 6669−6683.

(31) Griseri, M.; Tunca, B.; Huang, S.; Dahlqvist, M.; Rosén, J.; Lu, J.; Persson, P. O. Å.; Popescu, L.; Vleugels, J.; Lambrinou, K. Journal of the European Ceramic Society Ta-Based 413 and 211 MAX Phase Solid Solutions with Hf and Nb. *J. Eur. Ceram. Soc.* 2020, 40, 1829−1838.

(32) Ali, M. A.; Hossain, M. M.; Hossain, M. A.; Nasir, M. T.; Uddin, M. M.; Hasan, M. Z.; Islam, A. K. M. A.; Naqib, S. H. Recently Synthesized $(Zr_{1-x}Ti_x)_2AlC$ ($0 \leq x \leq 1$) Solid Solutions: Theoretical Study of the Effects of M Mixing on Physical Properties. *J. Alloys Compd.* 2018, 743, 146−154.

(33) Pan, R.; Zhu, J.; Liu, Y. Synthesis, Microstructure and Properties of $(Ti_{1-x}, Mo_x)_2AlC$ Phases. *Mater. Sci. Technol.* 2018, 34, 1064−1069.

(34) Kurakevych, O. O. Superhard Phases of Simple Substances and Binary Compounds of the B-C-N-O System: From Diamond to the Latest Results (a Review). *J. Superhard Mater.* 2009, 31, 139−157.

(35) Hadi, M. A.; Zahanggir Alam, M.; Ahmed, I.; Tanveer Karim, A. M. M.; Naqib, S. H.; Chroneos, A.; Islam, A. K. M. A. A Density Functional Theory Approach to the Effects of C and N Substitution at the B-Site of the First Boride MAX Phase Nb_2SB. *Mater. Today Commun.* 2021, 29, No. 102910.

(36) Gencer, A. First Principles Investigations of Ta_4AlX_3 (X= B, C, N) MAX Phase Ceramics. *J. Boron* 2020, 5, 115−123.

(37) Hossain, M. S.; Ali, M. A.; Hossain, M. M.; Uddin, M. M. Physical Properties of Predicted MAX Phase Borides Hf_2AB (A = Pb, Bi): A DFT Insight. *Mater. Today Commun.* 2021, 27, No. 102411.

(38) Rackl, T.; Johrendt, D. The MAX Phase Borides Zr_2SB and Hf_2SB. *Solid State Sci.* 2020, 106, No. 106316.

(39) Chakraborty, P.; Chakrabarty, A.; Dutta, A.; Saha-Dasgupta, T. Soft MAX Phases with Boron Substitution: A Computational Prediction. *Phys. Rev. Mater.* 2018, 2, No. 103605.

(40) Surucu, G. Investigation of Structural, Electronic, Anisotropic Elastic, and Lattice Dynamical Properties of MAX Phases Borides: An Ab-Initio Study on Hypothetical M_2AB (M = Ti, Zr, Hf; A = Al, Ga, In) Compounds. *Mater. Chem. Phys.* 2018, 203, 106−117.

(41) Ali, M. A.; Hossain, M. M.; Uddin, M. M.; Hossain, M. A.; Islam, A. K. M. A.; Naqib, S. H. Physical Properties of New MAX Phase Borides M_2SB (M = Zr, Hf and Nb) in Comparison with Conventional MAX Phase Carbides M_2SC (M = Zr, Hf and Nb): Comprehensive Insights. *J. Mater. Res. Technol.* 2021, 11, 1000−1018.

(42) Mitro, S. K.; Hadi, M. A.; Parvin, F.; Majumder, R.; Naqib, S. H.; Islama, A. K. M. A. Effect of Boron Incorporation into the Carbon-Site in Nb_2SC MAX Phase: Insights from DFT. *J. Mater. Res. Technol.* 2021, 11, 1969−1981.

(43) Gencer, A.; Surucu, G. Electronic and Lattice Dynamical Properties of Ti_2SiB MAX Phase. *Mater. Res. Express* 2018, 5, No. 076303.

(44) Surucu, G.; Gencer, A.; Wang, X.; Surucu, O. Lattice Dynamical and Thermo-Elastic Properties of M$_2$AlB (M = V, Nb, Ta) MAX Phase Borides. *J. Alloys Compd.* **2020**, *819*, No. 153256.

(45) Wang, J.; Ye, T. N.; Gong, Y.; Wu, J.; Miao, N.; Tada, T.; Hosono, H. Discovery of Hexagonal Ternary Phase Ti$_2$InB$_2$ and Its Evolution to Layered Boride TiB. *Nat. Commun.* **2019**, *10*, 1−8.

(46) Ade, M.; Hillebrecht, H. Ternary Borides Cr$_2$AlB$_2$, Cr$_3$AlB$_4$, and Cr$_4$AlB$_6$: The First Members of the Series (CrB$_2$)NCrAl with n = 1, 2, 3 and a Unifying Concept for Ternary Borides as MAB-Phases. *Inorg. Chem.* **2015**, *54*, 6122−6135.

(47) Kota, S.; Sokol, M.; Barsoum, M. W. A Progress Report on the MAB Phases: Atomically Laminated, Ternary Transition Metal Borides. *Int. Mater. Rev.* **2020**, *65*, 226−255.

(48) Ali, M. A.; Hadi, M. A.; Hossain, M. M.; Naqib, S. H.; Islam, A. K. M. A. Theoretical Investigation of Structural, Elastic, and Electronic Properties of Ternary Boride MoAlB. *Phys. status solidi* **2017**, *254*, 1700010.

(49) Ali, M. A.; Hossain, M. M.; Uddin, M. M.; Islam, A. K. M. A.; Naqib, S. H. Understanding the Improvement of Thermo-Mechanical and Optical Properties of 212 MAX Phase Borides Zr$_2$AB$_2$ (A = In, Tl). *J. Mater. Res. Technol.* **2021**, *15*, 2227−2241.

(50) Li, S.; Sun, W.; Luo, Y.; Yu, J.; Sun, L.; Wang, B.-T.; Liu, J.-X.; Zhang, G.-J.; Di Marco, I. Pushing the Limit of Thermal Conductivity of MAX Borides and MABs. *J. Mater. Sci. Technol.* **2022**, *97*, 79−88.

(51) Wang, Y. X.; Yan, Z. X.; Liu, W.; Zhou, G. L. Structure Stability, Mechanical Properties and Thermal Conductivity of the New Hexagonal Ternary Phase Ti$_2$InB$_2$ under Pressure. *Philos. Mag.* **2020**, *100*, 2054−2067.

(52) Ali, M. M.; Hadi, M. A.; Ahmed, I.; Haider, A. F. M. Y.; Islam, A. K. M. A. Physical Properties of a Novel Boron-Based Ternary Compound Ti$_2$InB$_2$. *Mater. Today Commun.* **2020**, *25*, No. 101600.

(53) Ali, M. A.; Hossain, M. M.; Uddin, M. M.; Islam, A. K. M. A.; Jana, D.; Naqib, S. H. DFT Insights into New B-Containing 212 MAX Phases: Hf$_2$AB$_2$ (A = In, Sn). *J. Alloys Compd.* **2021**, *860*, No. 158408.

(54) Ali, M. A.; Hossain, M. M.; Islam, A. K. M. A.; Naqib, S. H. Ternary Boride Hf$_3$PB$_4$: Insights into the Physical Properties of the Hardest Possible Boride MAX Phase. *J. Alloys Compd.* **2021**, *857*, No. 158264.

(55) Qureshi, M. W.; Ali, M. A.; Ma, X. Screen the Thermomechanical and Optical Properties of the New Ductile 314 MAX Phase Boride Zr$_3$CdB$_4$: A DFT Insight. *J. Alloys Compd.* **2021**, *877*, No. 160248.

(56) Segall, M. D.; Lindan, P. J. D.; Probert, M. J.; Pickard, C. J.; Hasnip, P. J.; Clark, S. J.; Payne, M. C. First-Principles Simulation: Ideas, Illustrations and the CASTEP Code. *J. Phys. Condens. Matter* **2002**, *14*, 2717−2744.

(57) Clark, S. J.; Segall, M. D.; Pickard, C. J.; Hasnip, P. J.; Probert, M. I. J.; Refson, K.; Payne, M. C. First Principles Methods Using CASTEP. *Z. Kristallogr. Cryst. Mater.* **2005**, *220*, 567−570.

(58) Perdew, J. P.; Burke, K.; Ernzerhof, M. Generalized Gradient Approximation Made Simple. *Phys. Rev. Lett.* **1996**, *77*, 3865−3868.

(59) Monkhorst, H. J.; Pack, J. D. Special Points for Brillouin-Zone Integrations. *Phys. Rev. B* **1976**, *13*, 5188−5192.

(60) Fischer, T. H.; Almlof, J. General Methods for Geometry and Wave Function Optimization. *J. Phys. Chem.* **1992**, *96*, 9768−9774.

(61) Hill, R. The Elastic Behaviour of a Crystalline Aggregate. *Proc. Phys. Soc. Sect. A* **1952**, *65*, 349−354.

(62) Ali, M. A.; Islam, A. K. M. A.; Ali, M. S. Ni-Rich Nitrides ANNi$_3$ (A = Pt, Ag, Pd) in Comparison with Superconducting ZnNNi$_3$. *J. Sci. Res.* **2011**, *4*, 1.

(63) Voigt, W.*Lehrbuch Der Kristallphysik*; Vieweg+Teubner Verlag: Wiesbaden, 1966. DOI: 10.1007/978-3-663-15884-4.

(64) Reuss, A. Berechnung Der Fließgrenze von Mischkristallen Auf Grund Der Plastizitätsbedingung Für Einkristalle. *ZAMM - J. Appl. Math. Mech./Zeitschrift für Angew. Math. und Mech.* **1929**, *9*, 49−58.

(65) Ali, M. A.; Roknuzzaman, M.; Nasir, M. T.; Islam, A. K. M. A.; Naqib, S. H. Structural, Elastic, Electronic and Optical Properties of Cu$_3$MTe$_4$ (M = Nb, Ta) Sulvanites — An *Ab Initio* Study. *Int. J. Mod. Phys. B* **2016**, *30*, 1650089.

(66) Ali, M. A.; Anwar Hossain, M.; Rayhan, M. A.; Hossain, M. M.; Uddin, M. M.; Roknuzzaman, M.; Ostrikov, K.; Islam, A. K. M. A.; Naqib, S. H. First-Principles Study of Elastic, Electronic, Optical and Thermoelectric Properties of Newly Synthesized K$_2$Cu$_2$GeS$_4$ Chalcogenide. *J. Alloys Compd.* **2018**, *781*, 37−46.

(67) Chen, Q.; Li, X.; Ye, B.; Xiong, L. First-Principle Prediction of Phase Stability, Electronic and Elastic Properties Study of the M$_{n+1}$AN$_n$ (A = Al, Si, M = Ti, Zr, Hf). *J. Phase Equilib. Diffus.* **2020**, *41*, 883−890.

(68) Khaledialidusti, R.; Khazaei, M.; Khazaei, S.; Ohno, K. High-Throughput Computational Discovery of Ternary-Layered MAX Phases and Prediction of Their Exfoliation for Formation of 2D MXenes. *Nanoscale* **2021**, *13*, 7294−7307.

(69) Ohmer, D.; Qiang, G.; Opahle, I.; Singh, H. K.; Zhang, H. High-Throughput Design of 211- M2AX Compounds. *Phys. Rev. Mater.* **2019**, *3*, No. 053803.

(70) Qureshi, M. W.; Ali, M. A.; Ma, X.; Tang, G.; Javed, M. U.; Paudyal, D. Verification of Stability and Unraveling the Electronic and Physical Properties of Bulk and (001)-Surfaces of Newly Synthesized Ti$_2$ZnX (X = C, N) MAX Phases. *Surf. Interfaces* **2022**, *31*, No. 102032.

(71) Qureshi, M. W.; Ma, X.; Tang, G.; Paudel, R. Ab Initio Predictions of Structure and Physical Properties of the Zr$_2$GaC and Hf$_2$GaC MAX Phases under Pressure. *Sci. Rep.* **2021**, *11*, 1−23.

(72) Dahlqvist, M.; Alling, B.; Rosén, J. Stability Trends of MAX Phases from First Principles. *Phys. Rev. B* **2010**, 220102.

(73) Atazadeh, N.; Saeedi Heydari, M.; Baharvandi, H. R.; Ehsani, N. Reviewing the Effects of Different Additives on the Synthesis of the Ti$_3$SiC$_2$ MAX Phase by Mechanical Alloying Technique. *Int. J. Refract. Hard Met.* **2016**, *61*, 67−78.

(74) Ali, M. A.; Islam, A. K. M. A. Sn$_{1−x}$Bi$_x$O$_2$ and Sn$_{1−x}$Ta$_x$O$_2$ (0≤x≤0.75): A First-Principles Study. *Phys. B* **2012**, *407*, 1020−1026.

(75) Ali, M. A.; Islam, A. K. M. A.; Jahan, N.; Karimunnesa, S. First-Principles Study of SnO under High Pressure. *Int. J. Mod. Phys. B* **2016**, *30*, 1650228.

(76) Ali, M. A.; Jahan, N.; Islam, A. K. M. A. Sulvanite Compounds Cu$_3$TMS$_4$ (TM = V, Nb and Ta): Elastic, Electronic, Optical and Thermal Properties Using First-Principles Method. *J. Sci. Res.* **2014**, *6*, 407−419.

(77) Born, M. On the Stability of Crystal Lattices I. *Math. Proc. Cambridge Philos. Soc.* **1940**, *36*, 160−172.

(78) Mouhat, F.; Coudert, F. X. Necessary and Sufficient Elastic Stability Conditions in Various Crystal Systems. *Phys. Rev. B* **2014**, *90*, No. 224104.

(79) Barsoum, M. W.; Radovic, M. Elastic and Mechanical Properties of the MAX Phases. *Annu. Rev. Mater. Res.* **2011**, *41*, 195−227.

(80) Kádas, K.; Iușan, D.; Hellsvik, J.; Cedervall, J.; Berastegui, P.; Sahlberg, M.; Jansson, U.; Eriksson, O. AlM$_2$B$_2$ (M = Cr, Mn, Fe, Co, Ni): A Group of Nanolaminated Materials. *J. Phys. Condens. Matter* **2017**, *29*, 155402.

(81) Chen, X.-Q.; Niu, H.; Li, D.; Li, Y. Modeling Hardness of Polycrystalline Materials and Bulk Metallic Glasses. *Intermetallics* **2011**, *19*, 1275−1281.

(82) Miao, N.; Sa, B.; Zhou, J.; Sun, Z. Theoretical Investigation on the Transition-Metal Borides with Ta$_3$B$_4$-Type Structure: A Class of Hard and Refractory Materials. *Comput. Mater. Sci.* **2011**, *50*, 1559−1566.

(83) Qin, Y.; Zhou, Y.; Fan, L.; Feng, Q.; Grasso, S.; Hu, C. Synthesis and Characterization of Ternary Layered Nb$_2$SB Ceramics Fabricated by Spark Plasma Sintering. *J. Alloys Compd.* **2021**, *878*, No. 160344.

(84) Bai, Y.; Sun, D.; Li, N.; Kong, F.; Qi, X.; He, X.; Wang, R.; Zheng, Y. High-Temperature Mechanical Properties and Thermal Shock Behavior of Ternary-Layered MAB Phases Fe$_2$AlB$_2$. *Int. J. Refract. Hard Met.* **2019**, *80*, 151−160.

(85) Li, N.; Bai, Y.; Wang, S.; Zheng, Y.; Kong, F.; Qi, X.; Wang, R.; He, X.; Duff, A. I. Rapid Synthesis, Electrical, and Mechanical Properties of Polycrystalline Fe$_2$AlB$_2$ Bulk from Elemental Powders. *J. Am. Ceram. Soc.* **2017**, *100*, 4407−4411.

(86) Wang, R.; Tao, X.; Ouyang, Y.; Chen, H.; Peng, Q. Suggest a New Approach to Fabricate AlFe$_2$B$_2$. *Comput. Mater. Sci.* **2020**, *171*, No. 109239.

(87) Li, X.-H.; Cui, H.-L.; Zhang, R.-Z. Structural, Optical, and Thermal Properties of MAX-Phase Cr_2AlB_2. *Front. Phys.* **2018**, *13*, 136501.

(88) Jhi, S. H.; Ihm, J.; Loule, S. G.; Cohen, M. L. Electronic Mechanism of Hardness Enhancement in Transition-Metal Carbonitrides. *Nature* **1999**, *399*, 132−134.

(89) Bouhemadou, A. Calculated Structural and Elastic Properties of M_2InC (M = Sc, Ti, V, Zr, Nb, Hf, Ta). *Mod. Phys. Lett. B* **2008**, *22*, 2063−2076.

(90) Bouhemadou, A. Structural, Electronic and Elastic Properties of Ti_2TlC, Zr_2TlC and Hf_2TlC. *Cent. Eur. J. Phys.* **2009**, *7*, 753−761.

(91) Hadi, M. A.; Kelaidis, N.; Naqib, S. H.; Chroneos, A.; Islam, A. K. M. A. Mechanical Behaviors, Lattice Thermal Conductivity and Vibrational Properties of a New MAX Phase Lu_2SnC. *J. Phys. Chem. Solids* **2019**, *129*, 162−171.

(92) Pugh, S. F. XCII. Relations between the Elastic Moduli and the Plastic Properties of Polycrystalline Pure Metals. *London, Edinburgh, Dublin Philos. Mag. J. Sci.* **1954**, *45*, 823−843.

(93) Pettifor, D. G. Theoretical Predictions of Structure and Related Properties of Intermetallics. *Mater. Sci. Technol.* **1992**, *8*, 345−349.

(94) Bai, Y.; Srikanth, N.; Chua, C. K.; Zhou, K. Density Functional Theory Study of Mn + 1AXn Phases : A Review Density Functional Theory Study of $M_{n+1}AX_n$ Phases : A Review. *Crit. Rev. Solid State Mater. Sci.* **2017**, 1−52.

(95) Kota, S.; Zapata-Solvas, E.; Ly, A.; Lu, J.; Elkassabany, O.; Huon, A.; Lee, W. E.; Hultman, L.; May, S. J.; Barsoum, M. W. Synthesis and Characterization of an Alumina Forming Nanolaminated Boride: MoAlB. *Sci. Rep.* **2016**, *6*, 26475.

(96) Hadi, M. A.; Christopoulos, S. R. G.; Naqib, S. H.; Chroneos, A.; Fitzpatrick, M. E.; Islam, A. K. M. A. Physical Properties and Defect Processes of M_3SnC_2 (M = Ti, Zr, Hf) MAX Phases: Effect of M-Elements. *J. Alloys Compd.* **2018**, *748*, 804−813.

(97) Ledbetter, H. M. Elastic Properties of Zinc: A Compilation and a Review. *J. Phys. Chem. Ref. Data* **1977**, *6*, 1181−1203.

(98) Wang, J.; Zhou, Y.; Liao, T.; Lin, Z. First-Principles Prediction of Low Shear-Strain Resistance of Al_3BC_3: A Metal Borocarbide Containing Short Linear BC2 Units. *Appl. Phys. Lett.* **2006**, *89*, No. 021917.

(99) Ranganathan, S. I.; Ostoja-Starzewski, M. Universal Elastic Anisotropy Index. *Phys. Rev. Lett.* **2008**, *101*, No. 055504.

(100) Ali, M. A.; Qureshi, M. W. DFT Insights into the New Hf-Based Chalcogenide MAX Phase Hf_2SeC. *Vacuum* **2022**, *201*, No. 111072.

(101) Ali, M. A.; Qureshi, M. W. Newly Synthesized MAX Phase Zr_2SeC: DFT Insights into Physical Properties towards Possible Applications. *RSC Adv.* **2021**, *11*, 16892−16905.

(102) Ali, M. A.; Hossain, M. M.; Jahan, N.; Islam, A. K. M. A.; Naqib, S. H. Newly Synthesized Zr_2AlC, $Zr_2(Al_{0.58}Bi_{0.42})C$, $Zr_2(Al_{0.2}Sn_{0.8})C$, and $Zr_2(Al_{0.3}Sb_{0.7})C$ MAX Phases: A DFT Based First-Principles Study. *Comput. Mater. Sci.* **2017**, *131*, 139−145.

(103) Ali, M. A.; Naqib, S. H. Recently Synthesized $(Ti_{1−x}Mo_x)_2AlC$ ($0 \leq x \leq 0.20$) Solid Solutions: Deciphering the Structural, Electronic, Mechanical and Thermodynamic Properties via Ab Initio Simulations. *RSC Adv.* **2020**, *10*, 31535−31546.

(104) Zhou, Y.; Sun, Z. Electronic Structure and Bonding Properties of Layered Machinable and Ceramics. *Phys. Rev. B* **2000**, *61*, 12570−12573.

(105) Scabarozi, T. H.; Amini, S.; Finkel, P.; Leaffer, O. D.; Spanier, J. E.; Barsoum, M. W.; Drulis, M.; Drulis, H.; Tambussi, W. M.; Hettinger, J. D.; Lofland, S. E. Electrical, Thermal, and Elastic Properties of the MAX-Phase Ti_2SC. *J. Appl. Phys.* **2008**, *104*, 1−6.

(106) Clarke, D. R. Materials Selection Guidelines for Low Thermal Conductivity Thermal Barrier Coatings. *Surf. Coat. Technol.* **2003**, *163–164*, 67−74.

(107) Surucu, G.; Yildiz, B.; Erkisi, A.; Wang, X.; Surucu, O. The Investigation of Electronic, Anisotropic Elastic and Lattice Dynamical Properties of MAB Phase Nanolaminated Ternary Borides: M_2AlB_2 (M=Mn, Fe and Co) under Spin Effects. *J. Alloys Compd.* **2020**, *838*, No. 155436.

(108) Belomestnykh, V. N.; Tesleva, E. P. Interrelation between Anharmonicity and Lateral Strain in Quasi-Isotropic Polycrystalline Solids. *Tech. Phys.* **2004**, *49*, 1098−1100.

(109) Mikitishin, S. I. Interrelationship of Poisson's Ratio with Other Characteristics of Pure Metals. *Sov. Mater. Sci.* **1982**, *18*, 262−265.

(110) Fine, M. E.; Brown, L. D.; Marcus, H. L. Elastic Constants versus Melting Temperature in Metals. *Scr. Metall.* **1984**, *18*, 951−956.

(111) Bouhemadou, A. Prediction Study of Structural and Elastic Properties under Pressure Effect of M_2SnC (M=Ti, Zr, Nb, Hf). *Phys. B* **2008**, *403*, 2707−2713.

(112) Salamon, D. Advanced Ceramics. In *Advanced Ceramics for Dentistry*; Elsevier Inc., 2014; pp. 103−122. DOI: 10.1016/B978-0-12-394619-5.00006-7.

(113) Cui, B.; Lee, W. E.; Cui, B.; Lee, W. E. High-Temperature Oxidation Behaviour of MAX Phase Ceramics. *Refract. Worldforum* **2013**, *5*, 105−112.

(114) Barsoum, M.; El-Raghy, T. The MAX Phases: Unique New Carbide and Nitride Materials. *Am. Sci.* **2001**, *89*, 334.

(115) Aydin, S.; Tatar, A.; Ciftci, Y. O. Some New Members of MAX Family Including Light-Elements: Nanolayered Hf_2XY (X= Al, Si, P and YCombining Double Low LineB, C, N). *Solid State Sci.* **2016**, *53*, 44−55.

(116) Li, S.; Ahuja, R.; Barsoum, M. W.; Jena, P.; Johansson, B. Optical Properties of Ti3SiC2 and Ti_4AlN_3. *Appl. Phys. Lett.* **2008**, *92*, 221907.

(117) Haddad, N.; Garcia-Caurel, E.; Hultman, L.; Barsoum, M. W.; Hug, G. Dielectric Properties of Ti_2AlC and Ti_2AlN MAX Phases: The Conductivity Anisotropy. *J. Appl. Phys.* **2008**, *104*, No. 023531.

(118) Rybka, M. *Optical Properties of MAX-Phase Materials*; M.Sc. Thesis, Linköping University: Sweden, 2009.

(119) Ali, M. A.; Ali, M. S.; Uddin, M. M. Structural, Elastic, Electronic and Optical Properties of Metastable MAX Phase Ti_5SiC_4 Compound. *Indian J. Pure Appl. Phys.* **2016**, *54*, 386−390.